

UNIVERSITÉ DU QUÉBEC À RIMOUSKI

**RECONSTITUTIONS PALÉOENVIRONNEMENTALES ET
PALÉOMAGNÉTIQUES À HAUTE RÉSOLUTION DE
SÉQUENCES SÉDIMENTAIRES PROVENANT DE LA BAIE
DE BAFFIN**

Mémoire présenté dans le cadre du programme de maîtrise en océanographie
en vue de l'obtention du grade de maître ès sciences

PAR
© MARIE-PIER ST-ONGE

Décembre 2012

UNIVERSITÉ DU QUÉBEC À RIMOUSKI
Service de la bibliothèque

Avertissement

La diffusion de ce mémoire ou de cette thèse se fait dans le respect des droits de son auteur, qui a signé le formulaire « *Autorisation de reproduire et de diffuser un rapport, un mémoire ou une thèse* ». En signant ce formulaire, l'auteur concède à l'Université du Québec à Rimouski une licence non exclusive d'utilisation et de publication de la totalité ou d'une partie importante de son travail de recherche pour des fins pédagogiques et non commerciales. Plus précisément, l'auteur autorise l'Université du Québec à Rimouski à reproduire, diffuser, prêter, distribuer ou vendre des copies de son travail de recherche à des fins non commerciales sur quelque support que ce soit, y compris l'Internet. Cette licence et cette autorisation n'entraînent pas une renonciation de la part de l'auteur à ses droits moraux ni à ses droits de propriété intellectuelle. Sauf entente contraire, l'auteur conserve la liberté de diffuser et de commercialiser ou non ce travail dont il possède un exemplaire.

Composition du jury :

Gwenaëlle Chaillou, président du jury, Université du Québec à Rimouski

Guillaume St-Onge, directeur de recherche, Université du Québec à Rimouski

Torsten Haberzettl, examinateur externe, Friedrich Schiller University of Jena

REMERCIEMENTS

Je remercie Guillaume St-Onge pour la direction de mon projet de maîtrise, pour son temps, sa disponibilité, sa confiance et pour sa capacité à transmettre sa passion. Merci aussi à Gwenaëlle Chailloux pour avoir accepté d'être la présidente de mon jury, et pour l'influence positive qu'elle a eue au courant de mes études. Merci à Torsten Haberzettl d'être mon évaluateur externe et pour l'enrichissement scientifique qu'il m'a apporté.

J'adresse mes remerciements aussi au capitaine, à l'équipage et aux scientifiques à bord du NGCC Hudson lors de l'expédition océanographique HU2008-029 dirigée par Calvin Cambell et Anne de Vernal et financée par la Commission géologique du Canada et le Conseil de recherches en sciences naturelles et en génie du Canada (CRSNG). Ce projet de maîtrise a été financé par une bourse de maîtrise du Fonds québécois de recherche en nature et technologies (FQRNT), une subvention du CRSNG, une subvention de recherche en équipe du FQRNT et une subvention du ministère du Développement économique, de l'Innovation et de l'Exportation (MDEIE) dans le cadre de la participation canadienne au projet européen *Past4future*.

Merci à Anne de Vernal pour les discussions enrichissantes et pour le soutien qu'elle m'a apporté. Merci à Anne Jennings pour le partage de ses données et sa disponibilité à répondre à mes questions.

Un merci du fond du cœur à Francesco Barletta, Quentin Simon, Manuel Bringué et Agathe Lisé-Pronovost pour les discussions et explications ainsi que pour leur constant

soutien et leur précieuse amitié. Merci à Jacques Labrie et à sa merveilleuse capacité à résoudre des problèmes. Merci à Yanick et Élie pour leur soutien et pour avoir cru en moi.

Et un merci spécial à Jean-Claude Soulard et Pierre Letarte pour avoir fait germer en moi cet esprit et cette rigueur scientifique qui m'accompagnent aujourd'hui.

RÉSUMÉ

Le but de cette recherche est de reconstruire, à l'aide des propriétés physiques et magnétiques du sédiment, les changements environnementaux ayant eu lieu au cours de l'Holocène. Quatre longues séquences sédimentaires (HU2008-029-034PC, -038PC, -042PC et -070PC) ont donc été prélevées au Nord (Smith Sound et Jones Sound) et à l'Est (Disko Bugt) de la Baie de Baffin. De plus, sur trois de ces quatre carottes, les variations millénaires à séculaires de l'orientation du champ magnétique ont été reconstituées puis comparées à d'autres enregistrements provenant de l'Ouest de l'Arctique. Les résultats montrent que les quatre carottes, qui couvrent une période maximale de 12360 a cal BP jusqu'à aujourd'hui, présentent des faciès sédimentaires qui correspondent aux grands changements climatiques de l'Holocène, c'est-à-dire, la déglaciation et le maximum thermique. De plus, sur deux carottes (HU2008-029-038PC et 070PC), les signaux de deux événements ayant une portée plus locale durant la période néoglaciaire ont été observés. Enfin, trois des quatre carottes (HU2008-029-034PC, -042PC et -070PC) ont présenté des propriétés magnétiques qui respectent les critères de qualité pour les enregistrements des variations d'orientation du champ magnétique terrestre. Les résultats ont donc été comparés avec d'autres carottes sédimentaires provenant de la mer de Chukchi et montrent que certaines variations millénaires à séculaires sont similaires de part et d'autre de l'Arctique canadien. Ce constat prend une place importante dans une meilleure compréhension du fonctionnement et du comportement du champ magnétique terrestre, spécialement dans l'Arctique. Cette découverte permet aussi une plus grande utilisation des résultats paléomagnétiques comme outil de chronostratigraphie.

Mots clés : Arctique, Baie de Baffin, Holocène, climat, paléomagnétisme, sédiment marin

ABSTRACT

The purpose of this research is to reconstruct, using the physical and magnetic properties of the sediment, environmental changes that occurred during the Holocene. Four long sediment sequences (HU2008-029-034PC, 038PC-, and-042PC - 070PC) have been taken in the North (Smith Sound and Jones Sound) and East (Disko Bugt) of Baffin Bay. In addition, three of the four cores were analyzed in order to reconstruct the paleomagnetic secular variation changes during the Holocene in Baffin Bay and compared to other records from the western Arctic. The results show that all four cores, which cover up to 12,360 cal yr BP until today, have sedimentary facies that correspond to major climate changes of the Holocene, i.e., deglaciation and the climatic optimum. In addition, for two cores (HU2008-029-038PC and 070PC), signals of two events during the Neoglacial period with a more local extent were observed. Finally, three of the four cores (HU2008-029-034PC, 042PC-and-070PC) have presented the magnetic properties that meet quality criteria for recording orientation variations of the geomagnetic field. The results have been compared with other sediment cores from the Chukchi Sea and show that some secular to millenia variations are similar at both sides of the Canadian Arctic. This observation took an important place in understanding the dynamic and behavior of the geomagnetic field, especially in the Arctic. This discovery also allows better use of paleomagnetic results as a chronostratigraphic use.

Keywords : Arctic, Baffin bay, Holocene, climate, paleomagnetism, marine sediment.

TABLE DES MATIÈRES

REMERCIEMENTS	VII
RÉSUMÉ	IX
ABSTRACT	XI
TABLE DES MATIÈRES	XIII
LISTE DES TABLEAUX	XVII
LISTE DES FIGURES.....	XIX
INTRODUCTION GÉNÉRALE.....	1
LA BAIE DE BAFFIN ET LES CHANGEMENTS CLIMATIQUES ACTUELS	1
LA CIRCULATION OCÉANIQUE DANS LA BAIE DE BAFFIN	3
L'HOLOCÈNE DANS LA BAIE DE BAFFIN	3
LE CHAMP MAGNÉTIQUE TERRESTRE ET LES PARTICULARITÉS DE L'ARCTIQUE ..	5
OBJECTIFS	6
LES PROPRIETES PHYSIQUES ET MAGNETIQUES DES SÉDIMENTS DE LA BAIE DE BAFFIN: UN ENREGISTREMENT DES CHANGEMENTS ENVIRONNEMENTAUX ET DES VARIATIONS PALEOMAGNETIQUES SECULAIRES AU COURS DE L'HOLOCENE.....	7
1.1 RÉSUMÉ EN FRANÇAIS DU PREMIER ARTICLE	7
1.2 PHYSICAL AND MAGNETIC PROPERTIES OF BAFFIN BAY SEDIMENTS: A RECORD OF ENVIRONMENTAL AND PALEOMAGNETIC SECULAR VARIATION CHANGES DURING THE HOLOCENE	9

ABSTRACT.....	9
INTRODUCTION.....	10
GEOLOGICAL AND ENVIRONMENTAL SETTING.....	11
The Holocene in Baffin Bay	14
Sediment facies in Baffin Bay	15
MATERIAL AND METHODS.....	16
Coring sites and core handling	16
Wet bulk density and low-field volumetric magnetic susceptibility.....	16
Diffuse spectral reflectance	17
Grain size	18
CAT-scan	18
Paleomagnetic analysis	18
Radiocarbon dating	20
Core top correlation.....	20
RESULTS	23
Lithostratigraphy, physical and magnetic properties	23
Natural remanent magnetization, magnetic mineralogy and grain size.....	29
CHRONOLOGY	33
ENVIRONMENTAL CHANGES DURING THE HOLOCENE AND SEDIMENT RESPONSE IN BAFFIN BAY	35
Site 34 – North Water Polynya	35
Site 38 – North Water Polynya	39
Site 42 – Jones Sound.....	40
Core 70 – Disko Bugt.....	43
PALEOMAGNETIC SECULAR VARIATIONS IN THE EASTERN AND WESTERN CANADIAN ARCTIC	45
CONCLUSIONS.....	49
ACKNOWLEDGEMENTS.....	49
REFERENCES.....	50

BACKGROUND DATASET	58
CONCLUSION GÉNÉRALE	63
RÉFÉRENCES BIBLIOGRAPHIQUES	65

LISTE DES TABLEAUX

Table 1. Coordinates and properties of the sampling sites.....	17
Table 2. Radiocarbon dates.....	21

LISTE DES FIGURES

Figure 1. Map of Baffin Bay and the location of the four coring sites. The bathymetric base map is from Ocean Data View. Surface currents are based on Melling et al. (2001) and Tang et al. (2004). NS is for Nares Strait, SS for Smith Sound and JS for Jones Sound.	12
.....
Figure 2. The continental shelf offshore Disko Bugt and the sampling location of core 70. From Weidick and Bennike (2007). The black arrows indicates the melt flow direction.	12
.....
Figure 3. Core top correlation for cores (A) 32BC, 34TWC and 34PC, (B) 40BC and 42PC, (C) 36BC, 38TWC and 38PC and (D) 68BC, 70TWC and 70PC. Open delta symbol represents the difference between each core. Colors illustrate the different sections.	.22
.....
Figure 4. Downcore physical and magnetic properties with CT-Scan images for core A) 34, B) 38, C) 42 and D)70.	26
.....
Figure 5. Downcore variations of inclination, declination, MAD values, MDF, pseudo-s ratio as well as the magnetic grain size indicator SIRM vs kLF for cores A) 34, B) 38, C) 42 and D) 70. The vertical line on the inclination graph indicates the expected GAD value for the latitude of each site. The magnetic grain size measurements also represented in a Day plot with their associated hysteresis curves. The arrows indicate where the u-channels were sub-sampled for the AGM measurements. The raw (red) and high-field slope corrected (black) magnetizations are illustrated. Red dots in the Day plots are associated with MD grains.	32
.....

Figure 6. Age model for cores A) 34, B) 38, C) 42 and D) 70. The depths were corrected for the missing sediments due to piston coring. Error bars reflect the 2σ ranges associated with the calibrated ages. Open symbols illustrate excluded ages.....	34
Figure 7. Downcore physical and magnetic properties with simplified lithology of cores A) 34, B) 38, C) 42 and D) 70.....	37
Figure 8. Comparison between the MDF profile of core 42 and key paleoceanographic proxies of core HLY03-05GC from Jennings <i>et al.</i> (2011). TU is for the transitionnal unit associated to the opening of Nares Strait observed in core HLY03-05GC. LM is for the Last Glacial Maximum.	42
Figure 9. Comparison of the magnetic susceptibility (blue squares) and density (black line) profiles of core 70 with temperature profiles from Weinick and Bennike (2007) and Dahl-Jensen <i>et al.</i> (1998) (ice core).	44
Figure 10. Comparison of inclination profiles between cores 34, 42 and 70 (this study) with cores from the eastern Canadian Arctic (Eastern Baffin bay stack; Andrews and Jennings, 1990) and western Canadian Arctic (HLY0501-08JPC; Lisé-Pronovost <i>et al.</i> , 2009, HLY0501-05; Barletta <i>et al.</i> , 2008). The original age scale of the Eastern Baffin Island stack from Andrews and Jennings (1990) was converted to calibrated ages.....	47
Figure 11. Comparison of the declination profiles between cores 34, 42 and 70 (this study) with cores from the western Canadian Arctic (HLY0501-08JPC; Lisé-Pronovost et al., 2009, HLY0501-05JPC; Barletta et al., 2008).	48

INTRODUCTION GÉNÉRALE

La baie de Baffin et les changements climatiques actuels

La baie de Baffin est un bassin entourant un rift datant du Crétacé (MacLean *et al.*, 1984). Le rift est entouré de demi-grabens plus récents qui se sont remplis de dépôts fluviaux deltaïques durant l'Éocène et le Pliocène (Li *et al.*, 2011). La partie centrale du bassin atteint des profondeurs allant jusqu'à 2300 mètres (Li *et al.*, 2011). Le plateau continental du côté ouest s'étend jusqu'à des profondeurs de 200-300 mètres avant d'atteindre le talus. Tandis que du côté Groenlandais, il atteint 400 à 500 mètres de profondeur (Li *et al.*, 2011).

Sur le plan océanographique, la baie de Baffin est un élément clé de la circulation thermohaline puisqu'elle est un des lieux de transfert d'eau froide et de glaces provenant de l'Arctique vers l'Atlantique Nord où il y aura formation d'eau profonde (Münchow *et al.*, 2006). C'est une baie aux multiples connexions : avec l'océan Atlantique par le détroit de Davis, avec l'Arctique principalement par le détroit de Nares, et avec l'archipel canadien par les détroits de Jones et Lancaster (figure 1). Mis à part la polynie des eaux du Nord, la baie de Baffin est recouverte de glace la majeure partie de l'année (Tang *et al.*, 2004).

La polynie des eaux du Nord est une région qui est libre de glace pendant la plus grande partie de l'année. Elle est générée par un *upwelling* provoqué par les vents du Nord (Levac *et al.*, 2001; Ingram *et al.*, 2002). L'*upwelling* entraîne la remontée de cellules d'eau plus chaude que la surface, créant un havre pour la faune et flore (Levac *et al.*, 2001; Ingram *et al.*, 2002). D'ailleurs, la Polynie des eaux du Nord est la région marine la plus productive au Nord du cercle Arctique (Barber *et al.*, 2001b). Les polynies sont des systèmes océanographiques complexes, mais d'un intérêt majeur dans l'étude du climat. En effet, la période de couvert de glace permet la séquestration du carbone absorbé par les

algues le reste de l'année. En contrepartie, la période libre de glace est associée à un albédo plus faible entraînant une rétroaction positive sur le réchauffement climatique (Barber *et al.*, 2001b). La sensibilité au climat de cet écosystème particulier pourrait être comparée, selon Barber *et al.* (2001a), au canari dans les mines de charbon en ce qui a trait aux changements climatiques actuels. Car une défaillance dans la dynamique des polynies, causée par les changements environnementaux actuels, serait un prélude à d'autres dysfonctionnements dans le système océanique global.

Une autre région de la baie de Baffin qui est d'un intérêt majeur pour l'étude du climat est Disko Bugt. C'est une baie d'approximativement 40 000 km² (Kelly et Lowell, 2009) dans laquelle se déversent les eaux de fonte et les icebergs du glacier *Jakobshavn Isbræ*. Celui-ci est alimenté par jusqu'à 6,5% de toute la glace du Groenland (Weidick et Bennike, 2007). Les glaciers du Groenland sont très sensibles aux variations climatiques et sont aussi vulnérables face au réchauffement climatique actuel (Gregory *et al.*, 2004; Hanna *et al.*, 2008). Les processus sédimentaires de Disko Bugt sont directement liés aux variations du glacier *Jakobshavn Isbræ*, et par conséquent, les changements climatiques. Lorsque les conditions environnementales diminuent l'impact du glacier sur les processus de déposition dans la baie, c'est le courant de l'Ouest du Groenland (*West Greenland Current* : WGC) qui prend la relève. D'ailleurs, dans les conditions actuelles, c'est le WGC qui domine la circulation océanique de la côte Ouest du Groenland (Lloyd *et al.*, 2007). Dans un scénario où le réchauffement climatique atteindrait une augmentation de 3°C au Groenland, la fonte des glaciers provoquerait une augmentation du niveau marin moyen de sept mètres pour une période d'au moins 1000 ans (Gregory *et al.*, 2004).

D'après ce que l'on sait actuellement des changements climatiques, si la tendance se maintient, l'Arctique sera libre de glace dans la seconde moitié du 21^e siècle (IPCC, 2007; Zhang et Walsh, 2006). C'est une région très sensible aux changements climatiques qui offre une vision accélérée du réchauffement de la planète. Le rapport de l'IPCC, en 2007, rapportait que l'augmentation des températures était deux fois plus importante en Arctique que la moyenne mondiale depuis les 100 dernières années (IPCC, 2007). De plus, la région

de la Baie de Baffin, plus spécifiquement le détroit de Lancaster, est en quelque sorte la porte d'entrée au passage du Nord-Ouest qui se situe dans l'Arctique canadien et américain (Pharand, 2007). Cette région est donc d'un intérêt majeur au niveau environnemental, politique et économique (Pharand, 2007).

La circulation océanique dans la Baie de Baffin

Tang *et al.* (2004) ont publié une étude basée sur une synthèse des données disponibles depuis 80 ans, en plus de leurs propres analyses et modélisations. Cette étude portait sur la variabilité de la circulation océanographique, des masses d'eau et de la présence des glaces de mer dans la baie de Baffin. Selon les auteurs, la baie de Baffin se compose de trois masses d'eau: les eaux de l'Arctique se situant dans les 100 à 300 premiers mètres de la baie, les eaux intermédiaires de l'Ouest du Groenland composant une couche située entre 300 et 800 mètres et les eaux profondes de la baie de Baffin présentent partout au-delà de 1200 mètres de profondeur (Tang *et al.*, 2004). Au Nord de la baie, particulièrement dans le détroit de Smith, la circulation est dominée par les eaux froides de l'Arctique qui descendent vers le Sud. À la hauteur de *Devon Island*, le courant Arctique rencontre le WGC. Celui-ci, après avoir remonté toute la côte Ouest du Groenland, est défléchi. Il tourne vers l'Ouest à la baie de Melville (*Qimusseriarsuaq*) puis redescend vers le Sud à partir de Cape York. La répartition verticale et horizontale des masses d'eau, ainsi que la force des courants, sont influencées par une variabilité annuelle et interannuelle (Tang *et al.*, 2004).

L'Holocène dans la Baie de Baffin

L'Holocène dans la baie de Baffin peut se diviser en trois grandes étapes liées à des changements environnementaux. Premièrement, les signatures sédimentaires associées à la déglaciation du Nord de la Baie de Baffin sont datées autour de 10900-10500 a cal BP (Knudsen *et al.*, 2008; Levac *et al.*, 2001). Toutefois, des indices d'une ré-avancée glaciaire de la calotte glaciaire Laurentidienne ont été observés entre 9500-9000 a cal BP sur l'Île de

Baffin (Miller *et al.*, 2005). La déglaciation s'accompagne d'un retrait progressif des glaces des calottes Laurentidienne et Groenlandaise du détroit de Nares vers 9000 a cal BP (Jennings *et al.*, 2011). Cela aurait permis la connexion entre l'Océan Arctique et l'Océan Atlantique et l'arrivée massive d'eau froide de l'Arctique dans la Baie de Baffin (Jennings *et al.*, 2011; Knudsen *et al.*, 2008; Levac *et al.*, 2001). Il n'y a pas de signature sédimentaire associée à cet évènement à Disko Bugt. Toutefois, le glacier *Jakobshavn Isbræ*, qui aurait atteint *Inner Egedesminde Dyb* (chenal) au maximum glaciaire, se serait progressivement retiré vers sa position actuelle pour laisser le WGC pénétrer l'intérieur de la baie et en contrôler les processus sédimentaires vers 7800 a cal BP (voir figure 2) (Lloyd *et al.*, 2005).

Des reconstitutions océanographiques basées sur des assemblages de dinokystes provenant de la baie de Baffin montrent que le climat se serait par la suite réchauffé pour atteindre ce que l'on nomme l'Optimum climatique Holocène. Cette période, où les températures de surface auraient été 3°C plus élevées par rapport à aujourd'hui, a eu un maximum vers 6000 a cal BP (de Vernal et Rochon, 2011). À Disko Bugt, cette période se serait étendue de 4000 à 8000 a cal BP (Weidick et Bennike, 2007).

Finalement, suite à l'Optimum climatique Holocène, il y a eu la période des néoglaciations (Weidick et Bennike, 2007; Jennings *et al.*, 2011; Lloyd *et al.*, 2005). Ce sont des épisodes de refroidissement climatique, mais de magnitude régionale. Les origines et les amplitudes des trois principaux épisodes de néoglaciation sont bien décrites dans l'article de Wanner *et al.* (2011). Le premier d'entre eux a eu lieu entre 3300 et 2500 a cal BP. Cet évènement froid coïncide avec une très faible activité solaire. Le deuxième, entre 1750 et 1350 a cal BP (AD 300-600) est aussi connu sous le nom de *Migration Period Cooling*. Ses origines sont encore discutées, mais des réavancées locales de glaciers ainsi que des signes de sécheresses ont été observés pour cette période. Enfin, le dernier événement, qui comprend aussi le Petit âge glaciaire, a eu lieu de 700 à 150 a cal BP (AD 1250-1800). Il est associé à un grand minimum dans l'activité solaire et à de nombreuses et fortes éruptions volcaniques tropicales. Certains auteurs (Mann *et al.*, 2009; Trouet *et al.*,

2009) avancent que cet épisode pourrait aussi être lié à un changement vers un mode négatif de l'oscillation Nord Atlantique (NAO). Selon Wanner *et al.* (2011), d'autres études seront nécessaires afin éclaircir les incertitudes liées aux mécanismes et à la chronologie des évènements climatiques holocène.

Le champ magnétique terrestre et les particularités de l'Arctique

L'échelle de temps basée sur la polarité géomagnétique est un outil fiable de stratigraphie pour les périodes de plusieurs centaines de milliers d'années. Sa découverte nous a aussi permis de mieux comprendre la dynamique du champ magnétique terrestre. Depuis les années 60, avec la découverte des anomalies magnétiques du plancher océanique, les recherches abondent pour peaufiner l'échelle des temps de polarité géomagnétique (voir la revue de littérature sur le sujet de Opdyke et Channell, 1996). Depuis les années 80, des recherches ont été entreprises sur les enregistrements sédimentaires afin d'approfondir les connaissances sur la géodynamo et la magnétostratigraphie. Ces travaux ont montré que la paléointensité relative mesurée dans des sédiments provenant de l'ensemble de la planète avait des variations communes et cohérentes à des échelles millénaire et même séculaire (Brachfeld, 2007; St-Onge *et al.*, 2003). Des compilations ont pu être réalisées afin de créer des courbes de référence, basées sur des enregistrements sédimentaires régionaux (e.g., Yamazaki et Oda, 2005; Stoner *et al.*, 2002; Gogorza *et al.*, 2004; Barletta *et al.*, 2010) et des modèles numériques (Korte *et al.*, 2005).

La région de l'Arctique reste une énigme. La dynamique et le comportement du champ magnétique terrestre dans le haut Arctique sont méconnus (St-Onge et Stoner, 2011). Des questions demeurent sur les similitudes et les différences observées sur le peu d'enregistrements prélevés en Arctique (Korte *et al.*, 2011). En les comparants à d'autres résultats provenant de plus basses latitudes, des théories peuvent naître sur le fonctionnement de la géodynamo et du champ magnétique terrestre (St-Onge et Stoner,

2011). Dans un contexte où le champ magnétique terrestre diminue d'intensité tout en se déplaçant à grande vitesse de l'Arctique canadien à la Sibérie (St-Onge et Stoner, 2011), il est primordial d'approfondir nos connaissances sur le comportement du champ magnétique terrestre dans l'Arctique.

Objectifs

Compte tenu de tous ces questionnements, les objectifs de cette maîtrise sont de (1) décrire et interpréter des unités sédimentaires associées à des changements environnementaux durant l'Holocène dans la baie de Baffin et (2) reconstruire et décrire la variabilité du champ magnétique terrestre enregistrée dans l'Arctique à partir de quatre carottes sédimentaires prélevées au Nord de la baie de Baffin et au large de la baie de Disko afin de placer les changements actuels dans un contexte temporel et géographique plus important.

CHAPITRE 1

LES PROPRIÉTÉS PHYSIQUES ET MAGNÉTIQUES DES SÉDIMENTS DE LA BAIE DE BAFFIN: UN ENREGISTREMENT DES CHANGEMENTS ENVIRONNEMENTAUX ET DES VARIATIONS PALÉOMAGNÉTIQUES SÉCULAIRES AU COURS DE L'HOLOCÈNE

1.1 RÉSUMÉ EN FRANÇAIS DE L'ARTICLE

Quatre longues séquences sédimentaires (HU2008-029-034PC, -038PC, -042PC et -070PC) ont été prélevées au Nord (Smith Sound et Jones Sound) et à l'Est (Disko Bugt) de la Baie de Baffin, dans le but de reconstruire, à l'aide des propriétés physiques et magnétiques du sédiment, les changements environnementaux ayant eu lieu au cours de l'Holocène. De plus, les variations millénaires à séculaires de l'orientation du champ magnétique ont été reconstituées et comparées à d'autres enregistrements provenant de l'Ouest de l'Arctique. Les datations au carbone 14 réalisées sur chacune des carottes montrent des vitesses de sédimentation allant jusqu'à 136 cm/ka. Les résultats montrent que les quatre carottes, qui couvrent une période maximale de 11850 a cal BP à aujourd'hui, présentent des faciès sédimentaires qui correspondent aux grands changements climatiques de l'Holocène, c'est-à-dire, la déglaciation et le maximum thermique. De plus, sur deux carottes (HU2008-029-038PC et 070PC), les signaux de deux événements ayant une portée plus locale durant la période néoglaciaire ont été observés. Enfin, trois des quatre carottes (HU2008-029-034PC, -042PC et -070PC) possèdent des propriétés magnétiques qui respectent les critères de qualité pour les enregistrements des variations d'orientation du champ magnétique terrestre. Les comparaisons avec d'autres carottes provenant de la mer de Chukchi montrent que certaines variations millénaires à séculaires sont similaires de part et d'autre de l'Arctique canadien. Cela suggère que le comportement du champ géomagnétique est similaire dans tout le Bas-Arctique, au moins jusqu'au 76°N.

Cet article intitulé « *Physical and magnetic properties of Baffin Bay sediments: a record of environmental and paleomagnetic secular variation changes during the Holocene* » a été corédigé par moi-même, le professeur Guillaume St-Onge et par la chercheure Anne Jennings. Comme première auteure, je me suis chargée de la recherche, de la méthodologie, de la réalisation de toutes les analyses, de l'interprétation des résultats et de la rédaction. Le professeur Guillaume St-Onge a eu l'idée originale, a supervisé les travaux et a contribué à la rédaction. Anne Jennings, troisième auteure, a effectué de nombreuses analyses radiocarbone et contribué à l'établissement de la chronologie des carottes.

L'article sera soumis prochainement dans un numéro spécial portant sur la baie de Baffin dans la revue internationale *Journal of Quaternary Science*. La forme de l'article ainsi que celle des figures, des tableaux et des références sont celles exigées par la revue.

1.2 Physical and magnetic properties of Baffin Bay sediments: a record of environmental and paleomagnetic secular variation changes during the Holocene

Marie-Pier St-Onge^{*1,2} and Guillaume St-Onge^{1,2}

¹Canada Research Chair in Marine Geology, Institut des sciences de la mer de Rimouski (ISMER), Université du Québec à Rimouski, Rimouski, Canada

²GEOTOP Research Center, Montreal, Canada

*Corresponding author: Marie-Pier St-Onge, marie-pier.st-onge@uqar.qc.ca

Keywords: Paleoceanography, deglaciation, climatic optimum, Neoglacial, paleomagnetic secular variations, Baffin Bay, Western Greenland, Disco Bugt

Paper submitted to the “*Baffin Bay and the NW Passage*” special issue of the Journal of Quaternary Science

ABSTRACT: The physical and magnetic properties of four long sediment cores (HU2008-029-034PC, -038PC, -042PC and -070PC) sampled in Northern (Smith Sound and Jones Sound) and Western (Disko Bugt) Baffin Bay were analyzed in order to reconstruct the environmental and paleomagnetic secular variation changes during the Holocene in Baffin Bay. The radiocarbon dating performed on each core revealed sedimentation rates up to 136 cm / ka. The results indicate that all four cores, which cover a period from 12360 a cal BP to present, have sedimentary facies that correspond to the major climatic changes of the Holocene: deglaciation and the climatic optimum. In addition, two cores (HU2008-029-038PC and -070PC), present the signal of two climatic events with a local influence during the Neoglacial period. Finally, three of the four cores

(HU2008-029-034PC, -042PC and -070PC) have magnetic properties that meet the criteria of quality for recording directional variations of the geomagnetic field. Comparison with other cores from the Chukchi Sea indicate that some millennial to secular variations are similar on both sides of the Canadian Arctic, suggesting that the geomagnetic field behavior is similar up to at least 76°N in the low Canadian Arctic.

Introduction

The Baffin Bay region is a very important component of current thermohaline circulation because it is a pathway for Arctic fresh waters and ice to the North Atlantic Ocean, which is a site of deepwater formation and thus contributing to the global oceanic circulation. Similarly, the northern part of Baffin Bay is an area of sea-ice production, icebergs and a pathway for cold Arctic waters to the Labrador Sea (Tang *et al.*, 2004; Holland *et al.*, 2001). This modern pattern of circulation in the North Atlantic Ocean took place during the Early Holocene, particularly with the opening of the Nares Strait at 9000 a cal BP (Jennings *et al.*, 2011). The connection between the Arctic and Atlantic Oceans most likely triggered local and global environmental changes, marked by associated sediment signatures. Many other climatic events, such as the Neoglacial period (Wanner *et al.*, 2011), may also have been recorded in this region.

The Disko Bugt area is also of special interest because of the proximity of the Jakobshavn Isbrae ice stream, which is one of the fastest ice streams in the world (Lloyd, 2006), and which drained ~6.5% of the Greenland Inland Ice (Weidick and Bennike, 2007). This is a key area for the recording of environmental changes associated with Greenland glaciers and the West Greenland Current, which is a mixture of the warm Irminger current and cold East Greenland current (Andersen, 1981; Ribergaard *et al.*, 2008; Tang *et al.*, 2004; Lloyd, 2006; Krawczyk *et al.*, 2010). Research on the influence of glaciers and current variations upon sediment response is crucial because it is very hard to find unequivocal evidence of sea-ice margins' response to specific climatic changes (Lloyd, 2006). Having

paleoceanographic data from the northern and southern Baffin Bay establishes whether the Holocene climatic events were of local or regional extent. The physical and magnetic properties of marine sediments can record these changes at a high temporal resolution. Combined with other proxies, like grain size, physical properties, benthic and planktonic foraminiferal assemblages and/or isotopic analysis, they can be used to describe and constrain climatic and environmental variations.

In addition, high-resolution paleomagnetic data from cores near the North Magnetic Pole are rare and can present a unique vantage point on Holocene geomagnetic field dynamics (St-Onge and Stoner, 2011). Moreover, comparing paleomagnetic results to others from the Arctic region may aid in understanding the magnitude of secular to millennial scale variations of the Earth's magnetic field during the Holocene (e.g., Barletta *et al.*, 2008; Sagnotti *et al.*, 2011; Lisé-Pronovost *et al.*, 2009; Korte *et al.*, 2011), allowing a better understanding of the geomagnetic field behavior in the Arctic as well as the development of an Arctic paleomagnetic dating tool (e.g., Barletta *et al.*, 2010; Antoniades *et al.*, 2011, Ólafsdóttir *et al.*, in press).

In this paper, we will (1) describe and interpret the sedimentary units associated with environmental variations during the Holocene in Northern Baffin Bay and offshore Disko Bugt regions, and (2) reconstruct paleomagnetic secular variations from these Arctic sites.

Geological and environmental setting

Baffin Bay is located between Northeastern Canada and Western Greenland (Fig. 1). It is 450 km wide and 1300 km long (Aksu and Piper, 1987), and it connects the Arctic and North Atlantic Oceans via Nares Strait, Lancaster Sound and Jones Sound (Tang *et al.*, 2004). Sediment transport is affected by fresh meltwater fluxes from land, icebergs, and seasonal pack ice (Perner *et al.*, 2011). The dominant current, consisting of cold Arctic waters, flows from West to East in the Jones Sound and from North to South in the Smith Sound (Tang *et al.*, 2004).

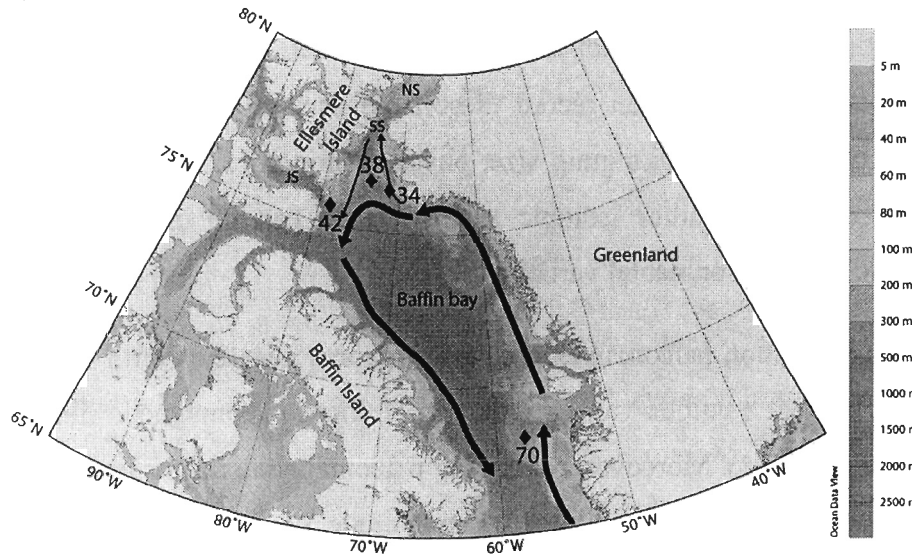


Figure 1. Map of Baffin Bay and the location of the four coring sites. The bathymetric base map is from Ocean Data View. Surface currents are based on Melling et al. (2001) and Tang et al. (2004). NS is for Nares Strait, SS for Smith Sound and JS for Jones Sound.

The northern part of the Baffin Bay can provide important paleoclimate data due to the meeting of the West Greenland Current (WGC) and polar waters from the Arctic Ocean (Knudsen *et al.*, 2008; Tang *et al.*, 2004). In addition, the northern part of Baffin Bay hosts the largest Canadian Arctic polynya. This 80,000 km² open water area is a result of the wind-driven upwelling of a warmer water layer: the Baffin Bay

Atlantic intermediate water (Knudsen *et al.*, 2008; Aksu, 1981). This polynya was established in the Early Holocene, ~9400 a cal BP (i.e., 9000 ¹⁴C a BP, Levac *et al.*, 2001). It is the most productive marine area north of the Arctic Circle (Barber *et al.*, 2001). The

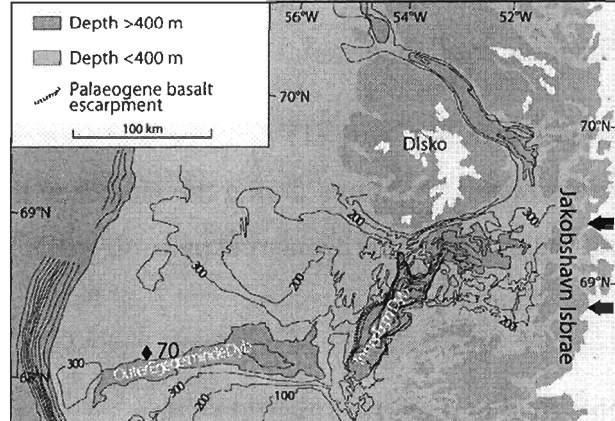


Figure 2. The continental shelf offshore Disko Bugt and the sampling location of core 70. From Weidick and Bennike (2007). The black arrows indicates the melt flow direction.

circulation inside the polynya is controlled by both the WGC and the Arctic Polar waters in a counter clockwise gyre (Melling *et al.*, 2001).

Disko Bugt is a large marine embayment, having a surface area of approximately 40,000 km² (Kelly and Lowell, 2009). The sampling site of core 70 (this study) is located northwest of Outer Egedesminde Dyb (valley) in a zone of intense iceberg scouring during the last glaciation (Weidick and Bennike, 2007) (Fig. 2). The sampling site was free of ice during the Last Glacial Maximum (LGM), which is very rare in the Holocene records for the region (Weidick and Bennike, 2007). Because it was unglaciated, it offers a vantage point for observing changes in sedimentation due to icebergs and the WGC.

Knudsen *et al.* (2008) described two cores (cores 008P and 012P), which are located very close to cores 38 and 34. The current at the site of core 38 is mostly controlled by Arctic Polar waters from Smith Sound (Tang *et al.*, 2004; Melling *et al.*, 2001), while circulation at the sampling site of core 34 is dominated by the WGC and a counter-current from Hvalsund Fjord (Knudsen *et al.*, 2008; Melling *et al.*, 2001).

The different intervals observed by Knudsen *et al.* (2008) in cores 008P and 012P allowed the depiction and dating of the different steps of deglaciation in northern Baffin Bay. Their interpretations are based on sediment facies, foraminifera, diatoms and stable isotope analysis. They have established seven distinct time intervals for core 008P and eight for core 012P. Moreover, Jennings *et al.* (2011) established the onset of the opening of Nares Strait at ~9000 a cal BP.

In the Disko Bugt area, studies by Hogan *et al.* (2011), Kelly and Lowell (2009), Weidick and Bennike (2007), Lloyd *et al.* (2005; 2007), and Johnsen *et al.* (2001) have identified several Holocene climatic events and in some cases, their sedimentary signatures. The sediment facies observed in the present study will be related to some of these events.

The Holocene in Baffin Bay

Deglaciation started at 15000 a cal BP in the Baffin Island area. Some readvances of the Laurentian Ice Sheet (LIS) and local glaciers have been dated to 9900-9500 a cal BP (Miller *et al.*, 2005). In Smith Sound, sediment signatures of the last deglaciation and extensive sea-ice cover have been observed until 10900 a cal BP by Knudsen *et al.* (2008) and 10500 a cal BP (9300 ^{14}C a BP) by Levac *et al.* (2001). After this period, planktonic productivity indicates an influence of the WGC in the region and warmer conditions (Knudsen *et al.*, 2008; Levac *et al.*, 2001).

At 9000 a cal BP, a major oceanographic event has occurred: the opening of Nares Strait, a pathway for Arctic waters entering Baffin Bay (Jenning *et al.*, 2011). After that, the presence of Arctic Polar waters has been observed in the microfossil flora assemblages in the area (Knudsen *et al.*, 2008).

For the Disko Bugt region, the Jakobshavn Isbrae icerstream position was near the basalt escarpment bordering the Inner Egedesminde Dyb (valley) until 11700 a cal BP (see Fig. 2; Weidick and Bennike, 2007). The presence of the WGC in the bay has been recorded starting at 10200 a cal BP (Lloyd *et al.*, 2005; Weidick and Bennike, 2007). The ice margin retreated to the eastern part of the bay, just west of the Jakobshavn fjord, until 9200 a cal BP. This new position of the meltwater and sediment source led to an increase in the influence of the WGC, particularly offshore. However, until 7800 a cal BP, the meltwater from Jakobshavn Isbrae, despite its retreat, deflected the warm current in the bay. Since then, the WGC has penetrated the bay, reflected by the presence of Atlantic waters microfauna (Lloyd *et al.*, 2005). According to Weidick and Bennike (2007), the western part of Egedesminde Dyb was unglaciated during the LGM.

During the Holocene, six global cold events (8200, 6300, 4700, 2700, 1550 and 550 a cal BP) have been triggered by different processes and recorded in lake/sea sediments, ice cores, speleothems, tree rings, peat bog sediments and fossil pollen records. Their structure and origin are well described in Wanner *et al.* (2011). Their influence, however, is not

recorded consistently on a regional scale, and often only local effects are observed. For example, except at a few sites from lakes in Baffin Island and the central Arctic (Miller *et al.*, 2005; Seppä *et al.*, 2003), there is no evidence from marine records of the 8200 a cal BP event in the High Arctic (Miller *et al.*, 2005).

Another important climatic event is the Holocene Thermal Maximum, which is a period of warm temperatures that have occurred around 6000 a cal BP in the northern Baffin Bay region (de Vernal and Rochon, 2011). Paleoceanographical reconstructions from dinocyst assemblages indicate that the sea-surface temperatures were 3°C higher than today (de Vernal and Rochon, 2011).

Sediment facies in Baffin Bay

Sediment deposits in high-latitude continental shelves are records of environmental changes related to the presence and proximity of ice (Hogan *et al.*, 2012). Dowdeswell *et al.* (1998) have presented a review of glacimarine sedimentary processes and facies for the Polar Atlantic region. The first facies associated with the last glaciation is a compact diamicton interpreted as subglacial till. In some of the cores analyzed, this is overlaid by a fine-grained lithofacies with varying degrees of laminations. It is interpreted as a deglaciation signal (Dowdeswell *et al.*, 1998). In others cores, the transition between diamicton and meltwater deposits comprises either pebbly diamictons interbedded with grey mud, or dropstones in soft grey muds. Then, a change from these laminated lithofacies to massive mud deposits represents the progression from ice proximal to ice distal conditions. As the ice retreated, the sediment flux decreased. Finally, fine hemipelagic sediments including possible IRD can be observed, indicating a period of no further meltwater influence on sediment deposition at the coring site (Aksu and Piper, 1987).

Material and methods

Coring sites and core handling

During the HU2008-029 oceanographic campaign in Baffin Bay, four piston cores (cores 034, 038, 042 and 070PC), their companion trigger weight cores (TWC) and associated box cores (BC) were collected on board the CCGS Hudson in 2008 (Fig. 1 and Table 1). Cores 034 and 038 were collected at water depths of 696 and 680 meters in the northern Baffin Bay polynya (Smith Sound). Core 042 was sampled at 580 meters in Jones Sound, whereas core 070 was raised offshore from Disko Bugt at a water depth of 444 meters (Fig. 1 and Table 1). The coring sites were determined using a Knudsen 3.5 kHz chirp sub-bottom profiler to identify areas with thick apparent Holocene sequences with the absence of mass movements and/or sediment perturbations. Composite depths have been established (see the core top correlation section) and the composite cores are named cores 34, 38, 42 and 70.

Once on board, the cores were cut into 1.5-m long sections and split lengthwise. They were then photographed at 500 dpi with a high-resolution Smart cube SmartCIS core scanner, then described and sampled with u-channels, rigid u-shaped plastic liners of 1.5 m length and 2 x 2 cm cross section. Trigger weight core HU2008-029-040 has no associated u-channel because the sediment was too watery for sampling. All cores were stored in a cold room at 4°C.

Wet bulk density and low-field volumetric magnetic susceptibility

Wet bulk density and low-field volumetric magnetic susceptibility (k_{LF}) were first measured on board on whole cores using a GEOTEK Multi Sensor Core Logger (MSCL) at

Table 1. Coordinates and properties of the sampling sites.

Cores	Latitude	Longitude	Location	Water depth	Lenght	Composite corrected lenght
	°N	°W		m	cm	cm
34	76.32905	71.418998	North water polynia	696	710	742
38	76.57349	73.955535	North water polynia	680	846	863
42	75.57939	78.629571	Jones Sound	580	1059	1112
70	68.22788	57.61746	Off Disko Bugt	444	250	431

1 cm and 0.5 cm intervals respectively for the piston cores and their companion trigger weight and box cores. k_{LF} was also measured on u-channels in the laboratory at 1 cm intervals using a point sensor. k_{LF} is an indicator of the concentration of ferrimagnetic material and is sensitive to variations in grain size (e.g., Stoner *et al.*, 1996; Thompson and Oldfield, 1986; Dearing *et al.*, 1999).

Diffuse spectral reflectance

Diffuse spectral reflectance was measured on board using a Minolta CM-2600d spectrophotometer at 0.5 cm intervals for the box and trigger weight cores and at 1 cm intervals for the piston cores. The spectral reflectance data are expressed in the CIE (International Commission on Illumination) L*, a*, b* color space which is often used in paleoceanography. L* ranges from black to white, a* from green to red and b* from blue to yellow (e.g., St-Onge *et al.*, 2007).

Grain size

Grain size measurements (0.04 to 2000 μm) were performed at 10 cm intervals in each core with a Beckman-Coulter LS13320 laser diffraction particle size analyzer at ISMER. The top and bottom of each core sections were also measured. Prior to the measurements, sediments were added to a Calgon electrolytic solution (sodium hexametaphosphate) and rotated for about 3 hours using an in-house rotator. The samples were then sieved (2 mm) and disaggregated in an ultrasonic bath for 90 s before their analysis. The particle size distribution output was then processed using the Gradistat software for sediment parameters (Blott and Pye, 2001).

CAT-scan

All core sections were passed through a computerized axial tomography-Scan (CAT-Scan) at INRS-ETE in Quebec City in order to characterize the sedimentary facies and sediment structures. It was notably used to determine the different sediment units, as well as to identify sediment deformation and shells for radiocarbon dating (see below).

Paleomagnetic analysis

All measurements were made at the Sedimentary Paleomagnetism and Marine Geology Laboratory of ISMER. Paleomagnetic data were measured on the u-channels at 1 cm intervals using a 2G Enterprises SRM-755 u-channel cryogenic magnetometer and pulse magnetizer module for Isothermal Remanent (IRM) and Saturated Isothermal Magnetizations (SIRM). Because of the response function of the magnetometer (e.g., Roberts, 2006; Weeks *et al.*, 1993) smoothing occurs due to the integration of empty space at the end and beginning of u-channels. The first and the last 4 cm of each section were thus excluded.

The natural remanent magnetization (NRM) was measured and then progressively demagnetized using stepwise peak alternating fields (AF) up to 80 mT at 5 mT increments. Declination and inclination of the characteristic remanent magnetization were calculated by

a least-square line-fitting procedure (Kirschvink, 1980) using the Mazaud (2005) software with AF demagnetization steps from 20 to 50 mT. Because the cores were not azimuthally oriented, the declination profiles are relative.

An anhysteretic remanent magnetization (ARM) was then induced using a 100 mT AF field with a 0.05 mT direct current (DC) biasing field. The ARM was measured and demagnetized up to 60 mT at 5 mT increments and then at 70, 80, 90 and 100 mT. Two isothermal remanent magnetizations were imparted with a DC field of 0.3 T (IRM 0.3 T) and 0.95 T (SIRM) with the pulse magnetizer module. Each IRM was demagnetized and measured at peak AF at 5 mT steps up to 60 mT, and also at 70, 80, 90 and 100 mT. SIRM was demagnetized and measured at 0, 10, 30, 50, 70, 90 and 120 mT.

Also presented in this paper are the Maximum Angular Deviation (MAD) values and the Median Destructive Field (MDF_{NRM}) of the NRM. MAD values under 5° are associated with very high-quality marine data (e.g., Stoner and St-Onge, 2007). The MDF_{NRM} , which is the value of the AF necessary to reduce the NRM intensity to half of its initial value, was also calculated with the Mazaud software. MDF values are dependent of the coercivity of magnetic minerals and magnetic grain size, and are a useful parameter in estimating magnetic mineralogy (e.g., Dankers, 1981). Also, the ARM_{20mT}/ARM_{0mT} ratio is a coercivity ratio that reflects variations in magnetic grain size if the mineralogy is dominated by low coercivity minerals such as magnetite (e.g., Andrews *et al.*, 2003).

Hysteresis measurements were performed on selected sediment samples in each core using a Princeton Measurement Corporation Micromag 2900 alternating gradient force magnetometer. Extracted from the hysteresis curves, the coercivity of magnetic minerals (H_c), the coercivity of remanence (H_{cr}), the saturation magnetization (M_s) and the saturation remanence (M_{rs}) were used to characterize the magnetic mineralogy and grain size (Day *et al.*, 1977).

Radiocarbon dating

The chronologies of the composite sequences of cores 34, 38, and 42 were determined using accelerator mass spectrometry (AMS) ^{14}C measurements at the Keck carbon cycle AMS facility, University of California, Irvine, CA, USA. The measurements on boxcore 40, which is associated to core 42, were made at the Lawrence Livermore National Laboratory, Livermore, CA, USA. Radiocarbon measurements for core 70 samples were made at the NSF-Arizona AMS Facility and the Scottish Universities Environmental Research Centre in the UK (Jennings *et al.*, this issue). Detailed data are presented in Table 2. The reported ages are in radiocarbon years using Libby's half-life of 5568 years and following the convention of Stuiver and Polach (1977). Conversion of conventional ^{14}C ages to calibrated years was made using the CALIB 6.0 online calibration software (Stuiver *et al.*, 2005) and the Hughen *et al.* (2004) marine dataset. The regional reservoir corrections used are indicated by a delta R in Table 1 and based on the online CALIB marine reservoir correction database. The calibrated ages are the median probability reported with a 1σ confidence level.

Core top correlation

Correlations between the piston cores and their associated trigger weight and box cores were conducted with the physical and magnetic properties in order to determine the sediment lost during piston coring (Fig. 3). Composite depths were then constructed for each site using the determined sediment lost. Diffuse spectral reflectance (a^*) and magnetic susceptibility were used to compare 32BC, 34TWC and 34PC. The correlation indicates a gap of 2 cm between the BC and TWC, and 34 cm between the TWC and PC. For core 42, a^* values indicate that there were 57 cm of missing sediments on the top of the piston core. There is only a 4 cm gap between the BC and TWC of core 38, as shown by the inclination and k_{LF} data, whereas comparison of the a^* and k_{LF} data between the TWC and PC indicates a difference of 19 cm. Inclination and declination data and L^* values were used to compare the BC, TWC and PC of core 70. There are 15 cm of missing sediment at the top.

Table 2. Radiocarbon dates. The numbers in parentheses represent the lower and the upper limits of a one sigma error range. Except for ages 8891 cal BP, 11038 cal BP and 11478 cal BP, of core 70, which have a error range of two sigma.

Cores HU2008-029	Section	Depth (cm)	Corrected depth U-channel (cm)	Dated material	Lab number	AMS ^{14}C age (yr BP)	ΔR	Calibrated age (cal BP)
34PC	DE	157	187	Pelecypod fragments	UCIAMS-61330	4265	171 +/- 23	(4048) 4140 (4220)
34PC	CD	280	304	Gastropod	UCIAMS-61331	5555	171 +/- 23	(5657) 5755 (5840)
38TWC	AB	167	180	Entire pelecypod shell	UCIAMS-61337	2585	171 +/- 23	(1972) 2050 (2126)
38PC	EF	195	212	Pelecypod fragments	UCIAMS-61333	3490	171 +/- 23	(3073) 3178 (3260)
38PC	DE	253	263	Entire pelecypod shell	UCIAMS-61335	3875	171 +/- 23	(3546) 3621 (3696)
38PC	CD	509	513	Pelecypod	UCIAMS-61340	5000	171 +/- 23	(5028) 5133 (5247)
38PC	CD	528	532	Pelecypod	UCIAMS-61339	5075	171 +/- 23	(5122) 5251 (5305)
38PC	CD	543	547	shell fragments	UCIAMS-61338	5115	171 +/- 23	(5221) 5285 (5366)
38PC	BC	586	587	Pelecypod fragments	UCIAMS-61341	5480	171 +/- 23	(5595) 5661 (5723)
38PC	AB	740	734	shell fragments	UCIAMS-61343	6425	171 +/- 23	(6636) 6702 (6774)
38PC	AB	801	795	shell fragments	UCIAMS-61342	7110	171 +/- 23	(7395) 7447 (7509)
40BC	Box core	24	24	shell fragments	CAMS-150983	810	252 +/- 29	(95) 195 (277)
40BC	Box core	42	42	shell fragments	CAMS-150984	975	252 +/- 29	(290) 366 (442)
42PC	DE	547	598	shell fragments	UCIAMS-61336	6305	252 +/- 29	(6397) 6468 (6547)
42PC	DE	571	622	Pelecypod valve	UCIAMS-61334	6505	252 +/- 29	(6635) 6701 (6773)
42PC	BC	766	810	Pelecypod	UCIAMS-61332	8155	252 +/- 29	(8317) 8367 (8413)
70TWC	BC	82-83	97	single valve <i>Arca glacialis</i>	AA84708	3197	140 +/- 30	(2754) 2828 (2876)
70TWC	BC	97-98	112	paired <i>Thyasira gouldi</i>	AA84709	3252	140 +/- 30	(2817) 2889 (2953)
70TWC	AB	134-135	149	seaweed	SUERC25670	5913	140 +/- 30	(6157) 6199 (6266)
70TWC	AB	172	187	paired <i>Macoma calcarea</i>	AA84710	7898	140 +/- 30	(8166) 8231 (8302)
70TWC	AB	194-195	210	seaweed	SUERC-3058	8464	140 +/- 30	(8695) 8891 (9022)
70PC	BC	14-15	190	seaweed	SUERC25672	7501	140 +/- 30	(7776) 7827 (7900)
70PC	BC	55-56	213	shell fragments	SUERC-3059	8830	140 +/- 30	(9309) 9368 (9429)
70PC	AB	142-144.5	318	fragments paired shell	AA84711	9831	140 +/- 30	(10502) 10551 (10592)
70PC	AB	169-170	345	paired small <i>Macoma crassula</i>	AA84712	10190	140 +/- 30	(10773) 10985 (11191)
70PC	AB	188-189	364	paired <i>Macoma calcalera</i>	AA84713	10174	140 +/- 30	(10796) 11038 (11164)
70PC	AB	209-211	385	large paired <i>Macoma calcalera</i>	AA84714	10545	140 +/- 30	(11246) 11478 (11711)

The first 161 cm are from the TWC and the rest is from the PC. Comparison of foraminifera assemblages yielded similar results for this core (Jennings *et al.*, this issue; Jennings and Walton, 2010).

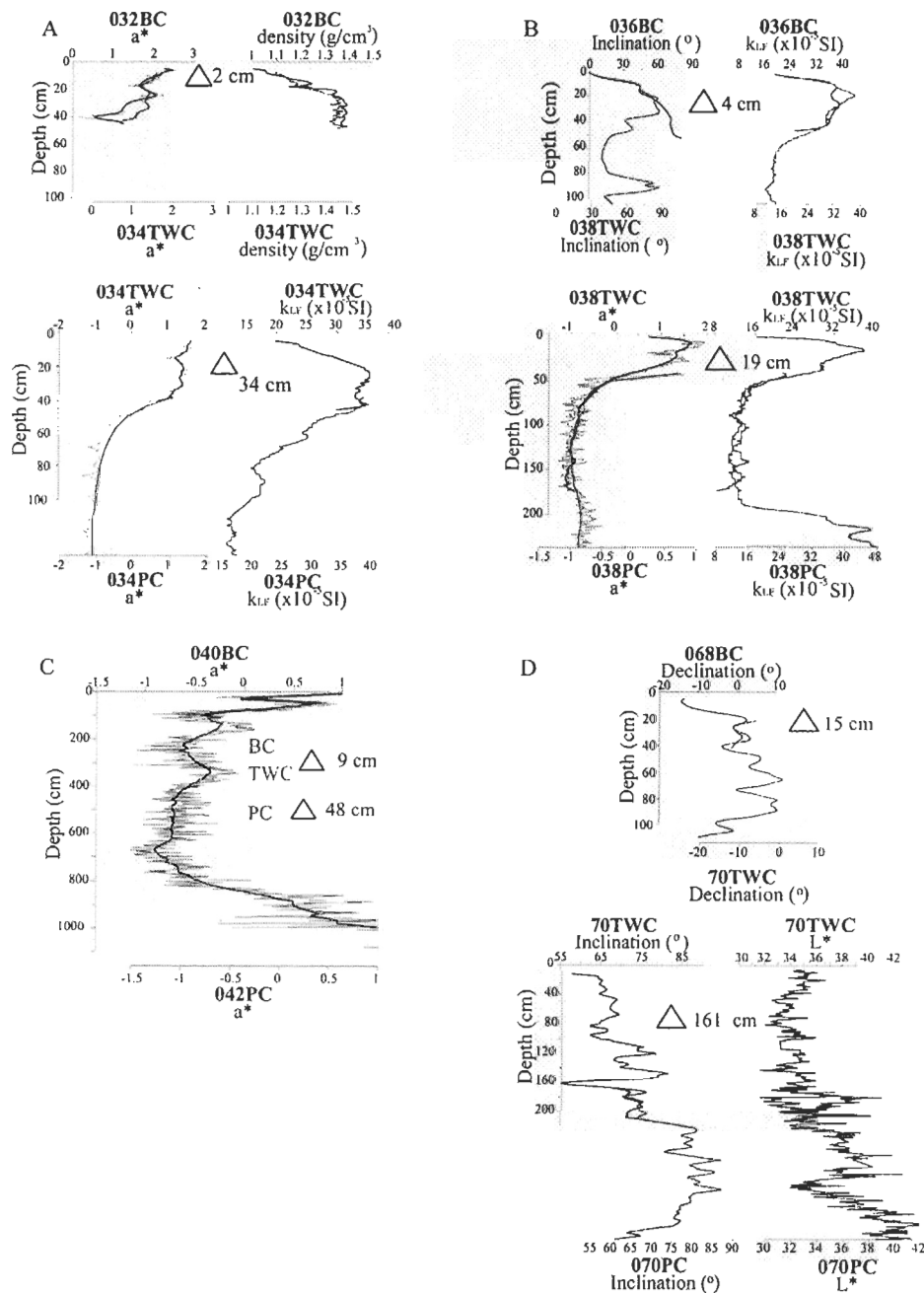


Figure 1. Core top correlation for cores (A) 32BC, 34TWC and 34PC, (B) 40BC and 42PC, (C) 36BC, 38TWC and 38PC and (D) 68BC, 70TWC and 70PC. Open delta symbol represents the difference between each core. Colors illustrate the different sections.

Results

Lithostratigraphy, physical and magnetic properties

Core 34

The physical and magnetic properties of core 34 allowed the identification of two distinct lithostratigraphic units (Fig. 4a). Unit 1, from 715 cm to 560 cm, is composed of a sequence characterized by two layers of reddish-brown sandy mud with pebbles and gravel. The coarser material present in both layers is reflected by higher values in density and magnetic susceptibility, and is visible on the CAT-scan images. Two peaks of magnetic susceptibility, with values reaching 200×10^{-5} SI, are observed and represent two distinct sub-units: 1a) and 1b). The first magnetic susceptibility peak in sub-unit 1a, around 615 cm, is coeval with the sparse accumulation of pebbles. The second sub-unit (sub-unit 1b: 715-640 cm) is a dense and compact reddish layer with laminations, sand, gravel and pebbles. This sub-unit is highlighted by a peak in L^* and a^* values. It is also marked by very low inclinations, sometimes even negative values (Fig. 5a). These low values in conjunction with the presence of coarse material and laminations indicate that this unit may be reflecting a rapidly deposited layer (e.g., St-Onge *et al.*, 2004; 2012).

Unit 2, from 560 cm to the top of the core, is composed of olive-grey (5Y4/2) and dark olive-grey (5Y3/2) silty clays. This unit is divided in four sub-units based on the presence of shell fragments and traces of bioturbation in sub-units a) and c). The density, magnetic susceptibility and magnetic remanence (NRM, ARM and IRM) profiles are relatively constant, but slightly increase to the bottom of the unit. On the other hand, an increase in MDF and ARM_{20mT}/ARM_{0mT} is observed from 110 cm to the top of the unit, indicating the presence of sediment with a higher coercivity and/or a decrease in magnetite grain size (e.g., Stoner and St-Onge, 2007; Andrews *et al.*, 2003), as no significant change in magnetic mineralogy can be deduced from the hysteresis loops and IRM/SIRM (Figs. 4 and

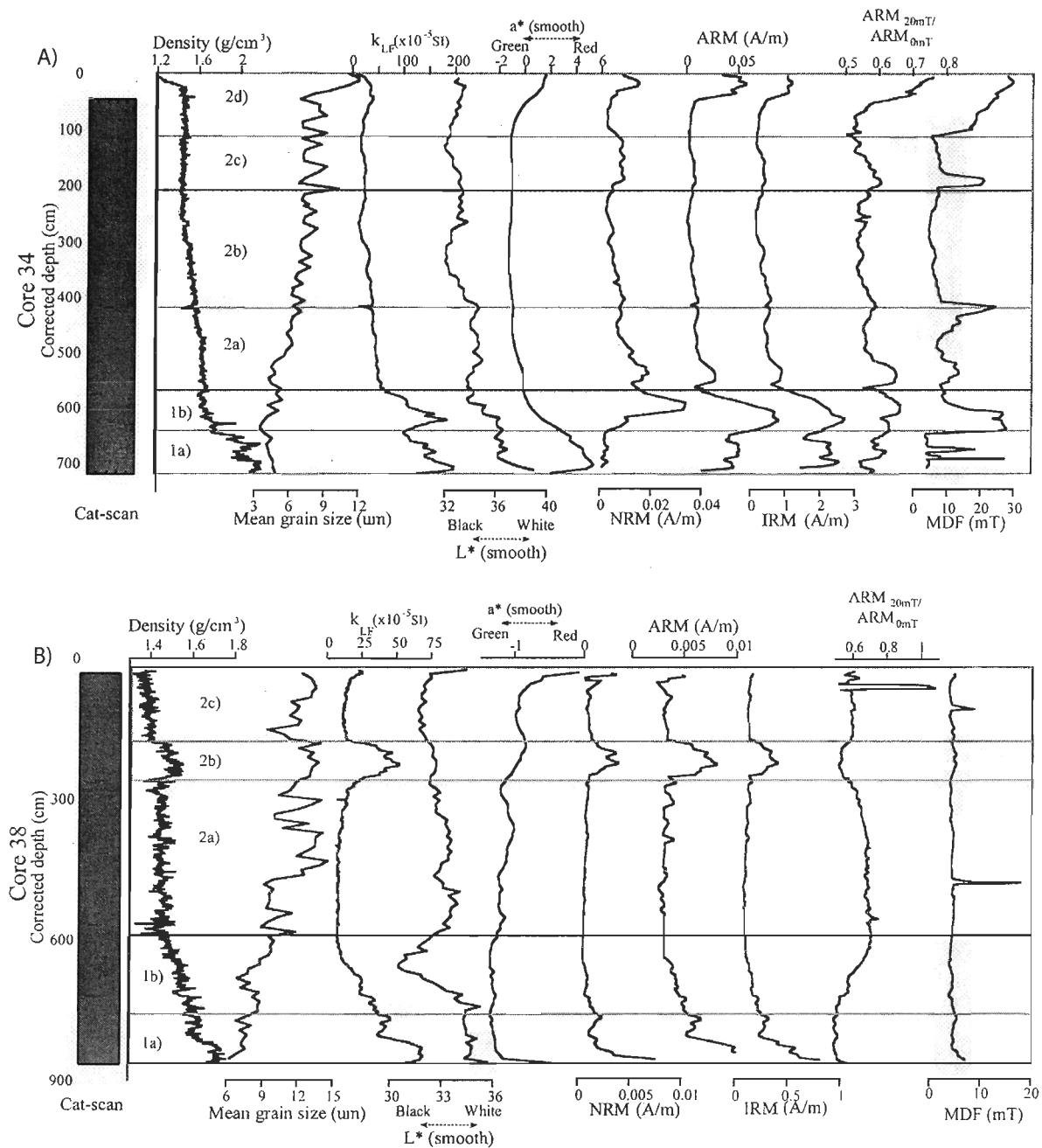
5). Furthermore, L* values, which are relatively constant in the entire unit, show a decrease starting around 60 cm to the top of the core.

Core 38

Core 38 is composed of olive-grey (5Y4/2) and dark olive-grey (5Y3/2) siltly clays (Fig. 4b). Except for two peaks at 483 cm and 110 cm, MDF values are low (mean of 4.62 mT) and constant, suggesting a uniform mineralogy with a combination of low coercivity and coarse magnetic grains. Based principally on the presence of shell fragments and traces of bioturbation, density, magnetic susceptibility and the magnetic properties (NRM, ARM and IRM), two main lithostratigraphic units were observed.

The first unit of core 38, from 860 cm to 505 cm, is characterized by an increase in magnetic susceptibility and density. This unit is also characterized by the presence of numerous shell fragments and traces of bioturbation (see background dataset). It should be highlighted that all the properties of this unit are constrained in the same range of values as sub-units 2a, 2b and 2c of core 34, possibly indicating a similar source and mode of deposition.

The second unit, from 505 cm to top of the unit, is characterized by very constant parameters. There are no significant traces of bioturbation or color changes. Sub-units a) and c) are very similar. Sub-unit 2b) contains some pebbles and shell fragments, as seen on CAT-scan images (see background dataset). Higher values of magnetic susceptibility, from 280 cm to 180 cm, are apparent and reach a maximum of 52×10^{-5} SI. Elevated values in the NRM, IRM and ARM profiles are also coeval with increased values of magnetic susceptibility, indicating a higher concentration of ferrimagnetic minerals. The lower values of $\text{ARM}_{20\text{mT}}/\text{ARM}_{0\text{mT}}$ in this interval indicate coarser magnetic grain size (e.g., Stoner and St-Onge, 2007; Andrews *et al.*, 2003) as no significant change in magnetic mineralogy can be deduced from the hysteresis loops and IRM/SIRM ratio (Figs. 4 and 5).



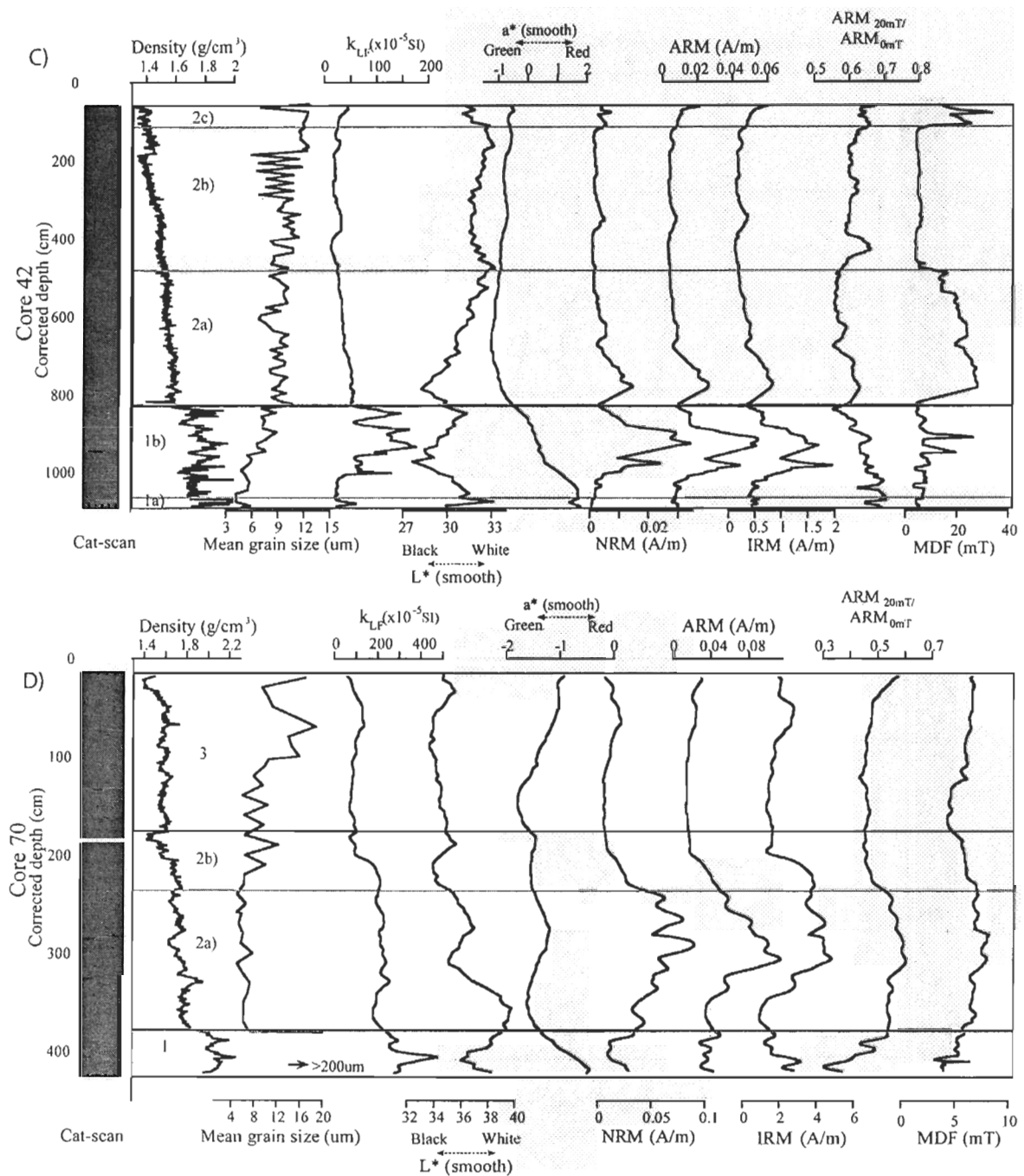


Figure 2. Downcore physical and magnetic properties with CT-Scan images for core A) 34, B) 38, C) 42 and D)70.

Core 42

In core 42, two lithostratigraphic units were defined according to density, magnetic susceptibility, color changes and the magnetic properties (NRM, ARM and IRM) (Fig. 4c). Most of the core is composed of olive-grey (5Y4/2) and dark olive-grey (5Y3/2) silty clays with a gradual color change to very dark brown (10YR2/2) starting at 980 cm.

Unit 1 is observed from 1087 cm to 835 cm. It is defined by a significant color change from the base to the top of the unit, passing from a^* values of +2 to -1. Magnetic susceptibility, NRM, ARM and IRM profiles indicate that deposition seems to have occurred in several steps. Peaks observed only in magnetic susceptibility data at 1080, 1000 and 845 cm, are associated with large pebbles that were not sampled in u-channels, but measured on the whole core analysis. High values in magnetic susceptibility, NRM, ARM and IRM between 950 and 880 cm are related to small pebbles present in the u-channels.

The unit has been divided in two sub-units. Sub-unit 1a), from 1087 to 1068 cm, is composed of compact clay with large pebbles. Sub-unit 1b), from 1068 to 835 cm, is characterized by the presence of numerous pebbles in a very dark brown silty clay with layers of sandy mud. There are a few intervals with laminations and normal grading that we interpret as turbidites. For a detailed view of this facies, please refer to the CAT-scan images in the background dataset.

Unit 2 of core 42, from 835 cm to the top of the core, is composed of very homogeneous and strongly bioturbated olive-grey (5Y4/2) and dark olive-grey (5Y3/2) silty clays. Shell fragments are present at the top of the core at 110 cm and 80 cm. The sub-units were determined using major changes in the MDF profile. Higher MDF values suggest that magnetic grains have a higher coercivity and/or a finer magnetic grain size if the mineralogy is constant. Sub-unit a) has higher MDF values than sub-unit b), with a decrease starting at 480 cm. Sub-unit c), from 105 to 63 cm, is characterized by relatively higher MDF values. The density and magnetic susceptibility values are very similar to the ones observed in unit 2 of core 34 and unit 1 of core 38.

Core 70

Three units were defined in core 70 based on the density and the magnetic properties (NRM, ARM, IRM, $\text{ARM}_{20\text{mT}}/\text{ARM}_{0\text{mT}}$ and MDF) (Fig. 4d). The first unit, from 417 cm to 375 cm, is composed of very dark gray (5Y 3/1) sands and the presence of numerous pebbles and shell fragments. It is associated with a peak of density, mean grain size, and magnetic susceptibility. Similarly, very low MDF and $\text{ARM}_{20\text{mT}}/\text{ARM}_{0\text{mT}}$ values most likely suggest a coarser magnetic grain size (e.g., Stoner and St-Onge, 2007; Andrews *et al.*, 2003), as the Day plot reveals a multi-domain magnetic grain size (Fig. 5d).

Unit 2 is observed from 375 cm to 175 cm. It is characterized by olive (5Y 4/3) and dark olive gray (5Y 3/2) siltly clays and by relatively higher magnetic property values (NRM, ARM, IRM, $\text{ARM}_{20\text{mT}}/\text{ARM}_{0\text{mT}}$ and MDF). Magnetic susceptibility reaches values around 200×10^{-5} SI in this unit, with a decrease at the top of the unit. Sub-unit 2b) is a transitional unit to unit 3. In sub-unit 2b, there are some traces of bioturbation. Toward its top, at 182 cm, there are a few laminations, whereas at the bottom of sub-unit 2a, a few pebbles are observed.

Unit 3 is a homogeneous olive-gray (5Y4/2) siltly clay unit with a few traces of bioturbation. All the parameters have lower values than in the rest of the core. However, the magnetic susceptibility values from this unit, ranging from 58 to 140×10^{-5} SI, are higher than in the other cores. From 70 to 60 cm, an interval of higher density is observed on the CAT-scan image. This interval is also characterized by normal grading and an increase in magnetic susceptibility values (max: 140×10^{-5} SI). We interpret this layer as a turbidite. Then, from 45 cm to the top of the core, an increase in a^* , L^* and $\text{ARM}_{20\text{mT}}/\text{ARM}_{0\text{mT}}$ is observed.

Natural remanent magnetization, magnetic mineralogy and grain size

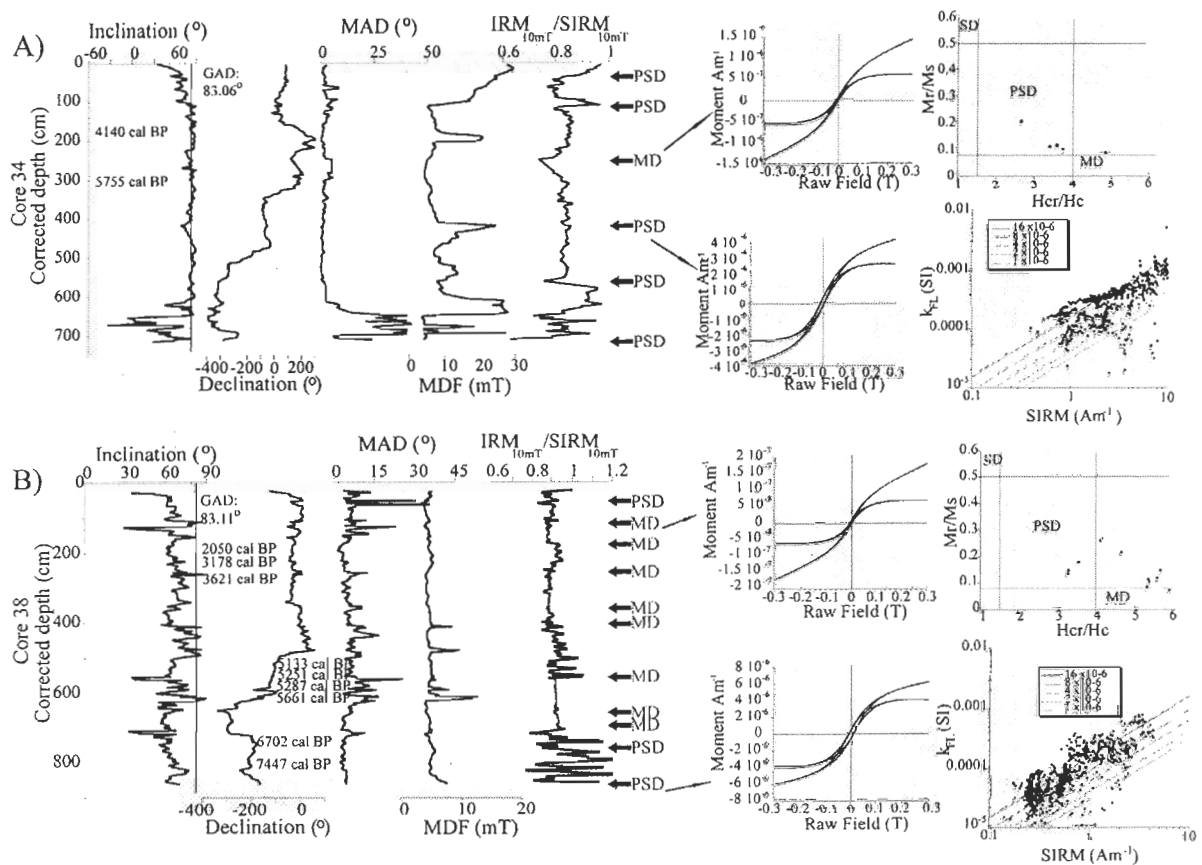
Hysteresis curves of the discrete samples from all cores (Fig. 5) indicate that low coercivity minerals such as magnetite in the pseudo-single to multi domain ranges are the dominant magnetic carrier (e.g., Tauxe, 2010). Similarly, day plots (Day *et al.*, 1977) indicate that most of the sediments of the four cores are composed of pseudo-single domain (PSD) magnetic grains, except for core 38 which contains coarser multi domain magnetite grains (MD) (Fig. 5b). Moreover, Mrs/Ms values ranging between 0.1 and 0.3 are characteristic of magnetite/titanomagnetite grains (Day *et al.*, 1977; Tauxe, 1993).

The k_{LF} /SIRM diagram indicates that for most of cores 34 (Fig. 5a), 42 (Fig. 5b) and 70 (Fig. 5c), there is a scattered distribution of magnetic grain sizes, including larger multi domain grains in cores 34 and 70. For core 34, this highlighted interval corresponds to 110–300 cm, but does not include the peak in MDF values between 204 and 181 cm. It is not related to a specific lithofacies, but it can be associated with low (<0.6) ARM_{20mT}/ARM_{0mt} values. Regarding core 70, this interval of multi-domain grains corresponds to 424–310 cm. It is related to a decrease in magnetic parameter values (NRM, ARM, IRM, ARM_{20mT}/ARM_{0mT} and MDF) from 390 to 292 cm, and to the presence of coarser sediment in unit 1.

As a whole, the inclination data fluctuate around the expected inclination for the latitude of each site based on a geocentric axial dipole (GAD) model. However, core 38 and part of core 70 have lower inclinations than the ones expected based on a GAD. For core 38, the deviation from the GAD value is associated with lower NRM (Tauxe and Kent, 2004) and MDF values. Indeed, except for sub-unit 2b and the base of the core 38, the NRM mean value is 0.0007 A/m. This is one order of magnitude lower than the NRM of cores 34 and 42. For the upper part of core 70, the lower inclination values were most likely caused by coring deformation. Nonetheless, excluding the intervals mentioned above for cores 34, 42 and 70 (less than 14% for core 34, 12% for core 42, and 4% for core 70) and for most of core 38, the MAD values are below 10°, still indicative of well-defined paleomagnetic directional data (e.g., Stoner and St-Onge, 2007). In addition, the pseudo S ratio in cores 42

and 70, with mean values of 0.96 and 0.94, suggests that magnetite is the dominant magnetic carrier. Cores 34 and 38, which are located in the North Water Polynya, have lower pseudo S ratio mean values of 0.84 and 0.91 respectively, but are still indicative of the dominance of low coercivity minerals such as magnetite. The MDF for cores 42, 34, 38, and 70 respectively ranges from 5 to 30 mT, 5 to 30 mT, 5 to 20 mT, and 5 to 10 mT. These relatively low MDF values, in conjunction with pseudo S ratios indicative of magnetite, suggest that the sediment has a low coercivity probably due to coarser magnetic grain sizes. Similar lower MDF values were also observed in the Chukchi Sea and were associated with coarser grains of magnetite (Lis  -Pronovost *et al.*, 2009).

In brief, these data indicate that, excluding the specific intervals discussed above, the four cores are characterized by a strong, stable and single component magnetization (see background dataset) and that the magnetic remanence is most likely carried by low coercivity minerals such as magnetite in the PSD range. Nonetheless, in some intervals and for the most part of core 38, MD grains are observed. Consequently, all these results indicate that, except for core 38, most of the sediments of the three other cores (cores 34, 42 and 70) are suitable for the recording of coherent paleomagnetic directional data. As a result, only the directional data of these three cores will be further discussed.



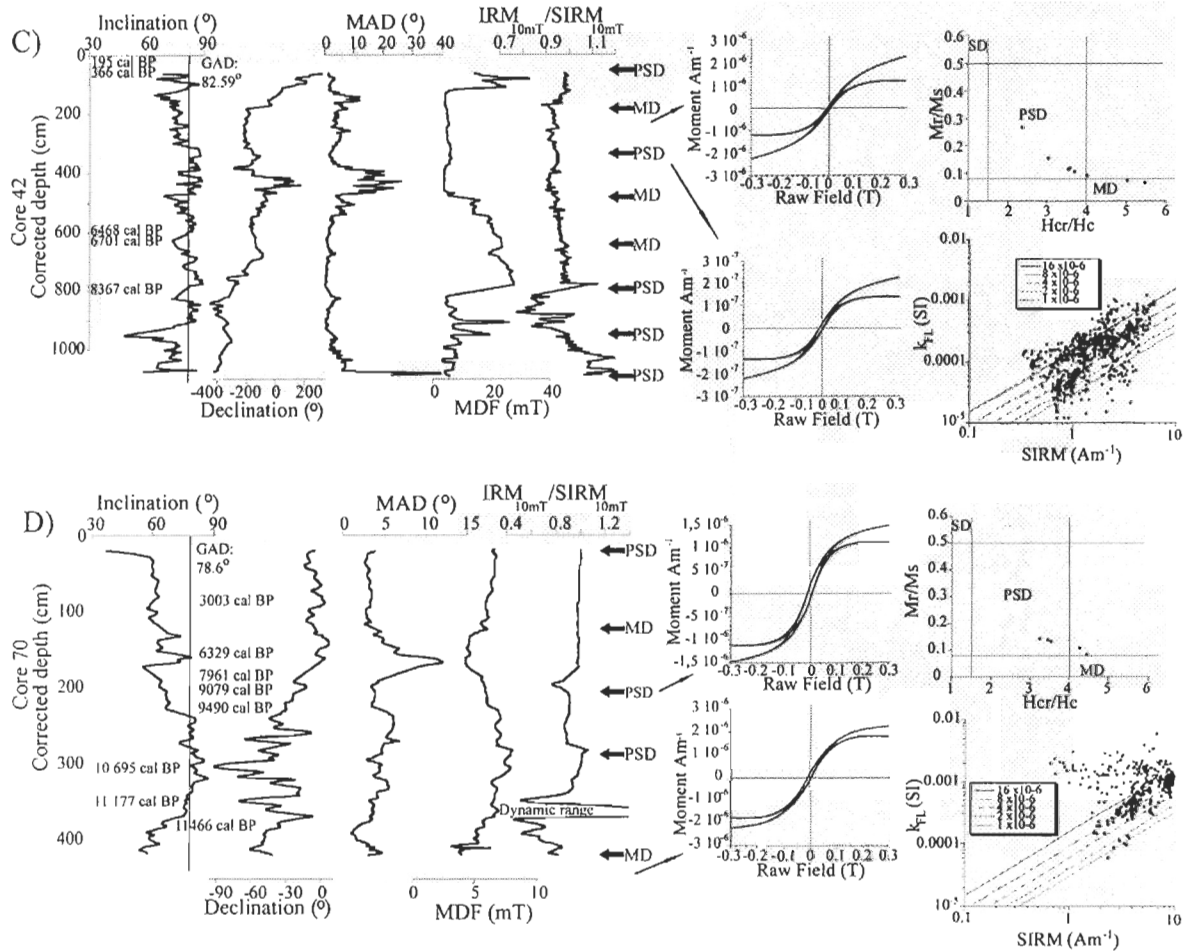


Figure 3. Downcore variations of inclination, declination, MAD values, MDF, pseudo-s ratio as well as the magnetic grain size indicator SIRM vs kLF for cores A) 34, B) 38, C) 42 and D) 70. The vertical line on the inclination graph indicates the expected GAD value for the latitude of each site. The magnetic grain size measurements also represented in a Day plot with their associated hysteresis curves. The arrows indicate where the u-channels were sub-sampled for the AGM measurements. The raw (red) and high-field slope corrected (black) magnetizations are illustrated. Red dots in the Day plots are associated with MD grains.

Chronology

The four radiocarbon-based age models are presented in Figure 6. Because the four cores have different sedimentation rate, four different methods have been used to establish the age models. The age model for core 34 was constructed with a linear interpolation between available ages. There are two different sedimentation rates: 76 cm/ka from the base to 4000 a cal BP and 46 cm/ka from 4000 a cal BP to the top. The age model of core 38 was constructed using a linear interpolation for the top of the core and a fifth degree polynomial fit for the rest of the core. The sedimentation rate is 136 cm/ka for the base of the core, 31 cm/ka for the plateau between 2000 and 4000 a cal BP, and 85 cm/ka for the top of the core. For core 42, the age model was constructed with a simple linear interpolation between all the calibrated ^{14}C ages. The mean sedimentation rate is 46 cm/ka. Finally, for core 70, a fifth degree polynomial fit was established. There are two different sediment rates for this part of the core: 75 cm/ka for the base of the core and 20 cm/ka from ~9000 to ~3000 a cal BP. The top of the age model was constructed using a linear relationship between the first two ages, yielding a sedimentation rate of 32 cm/ka.

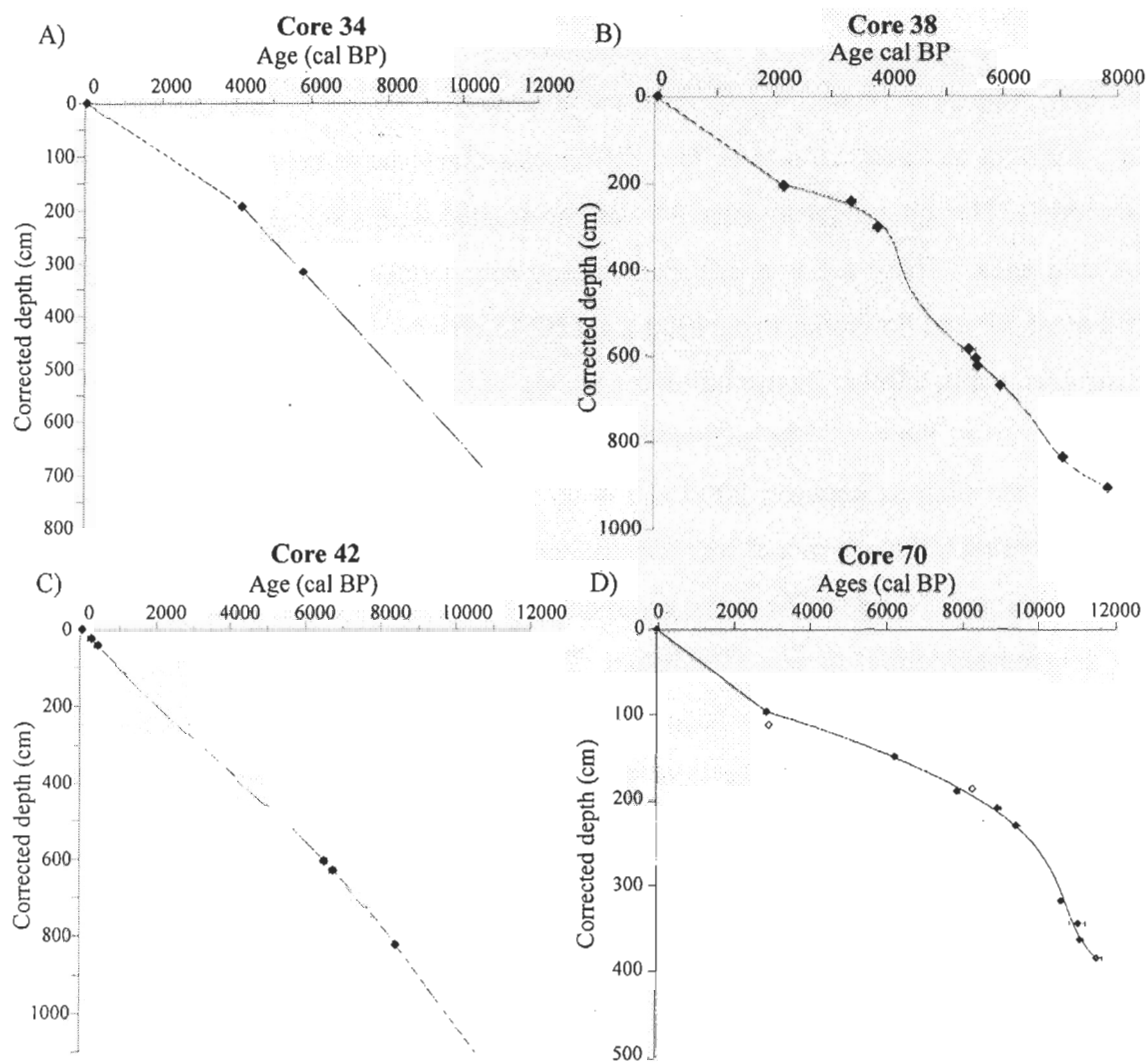


Figure 4. Age model for cores A) 34, B) 38, C) 42 and D) 70. The depths were corrected for the missing sediments due to piston coring. Error bars reflect the 2σ ranges associated with the calibrated ages. Open symbols illustrate excluded ages.

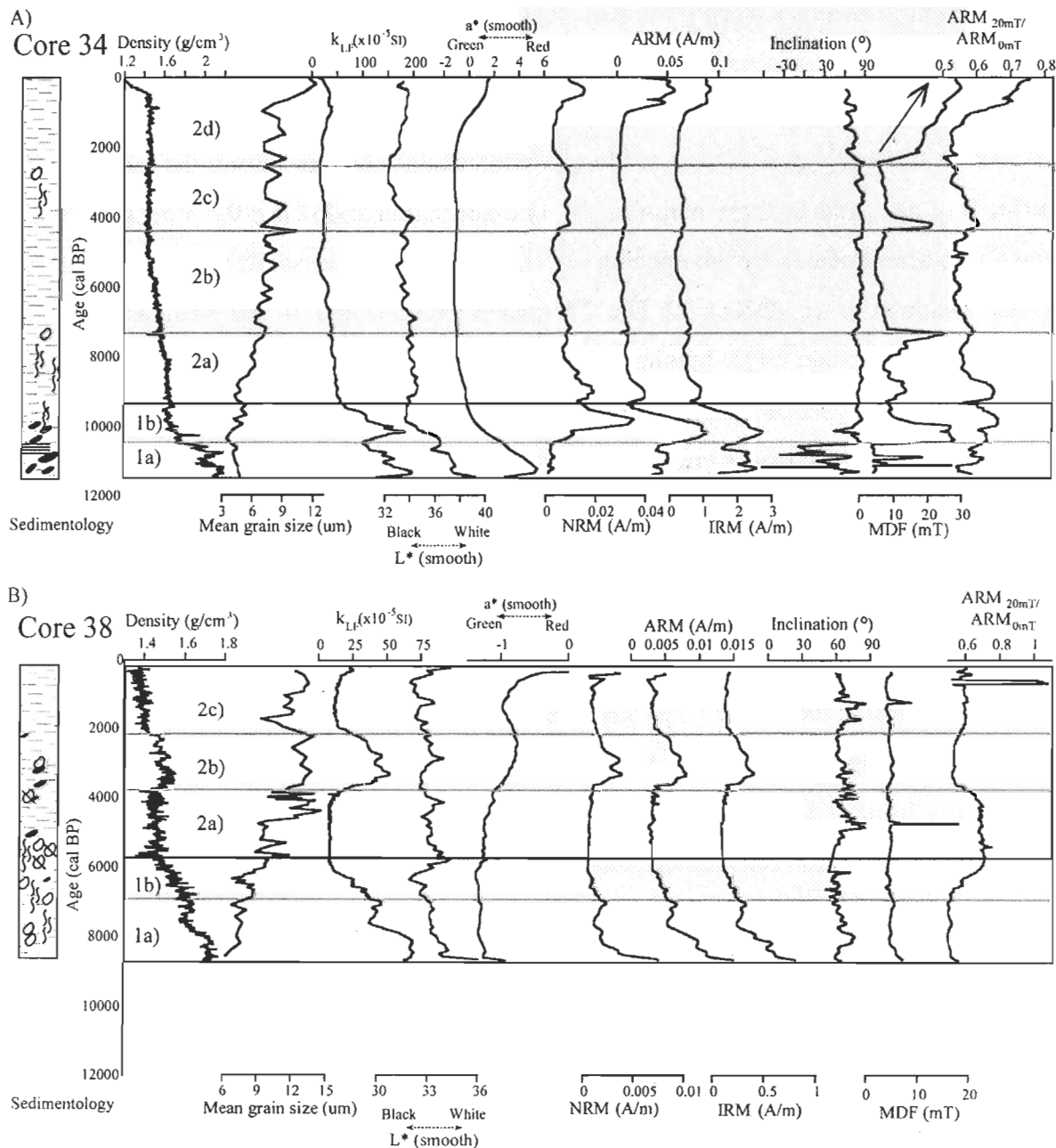
Environmental changes during the Holocene and sediment response in Baffin Bay

As seen in the geological setting section, environmental changes during the Holocene in Baffin Bay occurred in three major steps: 1) deglaciation following the Younger Dryas, which was accompanied by the opening of Nares Strait, dated at approximately 9000 a cal BP by Jennings *et al.* (2011), 2) The Thermal Maximum and 3) the Neoglacial period (Weidick and Bennike, 2007; Jennings *et al.*, 2011; Lloyd *et al.*, 2005). The timing of these main changes is variable because strong inter-regional contrasts could have occurred (Roberts, 2002). Moreover, some local events have not been recorded in all cores. Below, we present the interpretation of the different sediment facies described in the results section. Global and local environmental events are linked to those sediment signatures.

Site 34 – North Water Polynya

Core 34 is located very close (55 km directly to the South) to core 012P, previously analyzed by Knudsen *et al.* (2008), though they were not recovered from the same sedimentary basin. Core 34 was sampled in Smith Sound and core 012P in Hvalsund (a Greenland fjord), which can explain some differences between their sediment signatures.

The two cores nonetheless show several similarities. The first sub-unit of core 34 (Fig. 7a) is very similar to intervals 1, 2 and 3 of core 012P of Knudsen *et al.* (2008). The authors described the first interval as a reddish diamicton layer and interpreted it as a till. This interval is followed by two intervals of laminated clay and silty-clay. The mode of deposition is interpreted to be in turbulent waters and seasonal sedimentation from meltwater plumes. The sediment descriptions and the stratigraphic position of the intervals and sub-units in cores 34 and 012P are almost identical, but there are significant differences related to the chronology of these units. Sub-unit 1a) ranges from 10500 to 11400 a cal BP, compared to >12500 to 11300 a cal BP for the three intervals described in Knudsen *et al.*



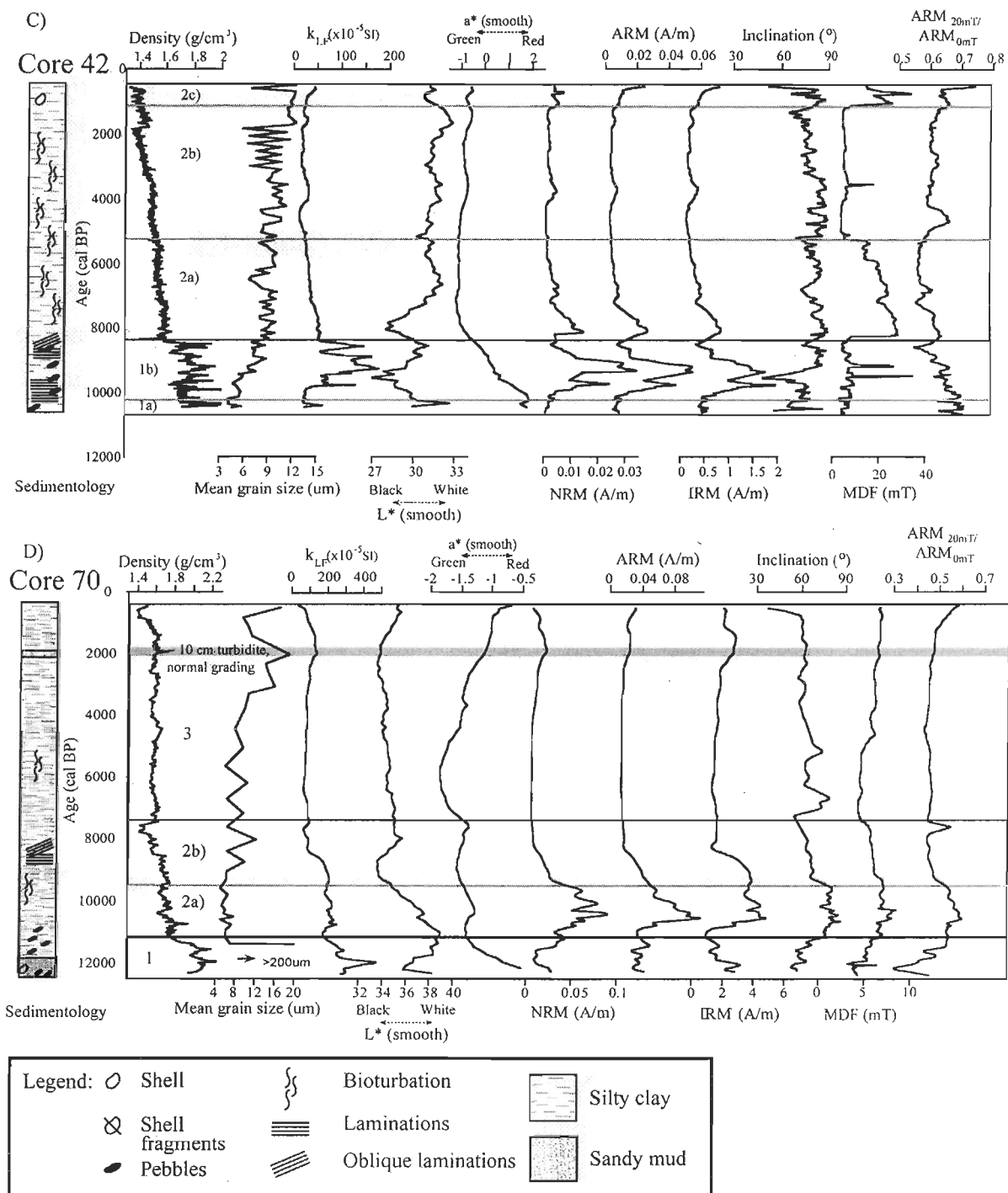


Figure 5. Downcore physical and magnetic properties with simplified lithology of cores A) 34, B) 38, C) 42 and D) 70.

(2008). This difference is likely the result of the chronology of core 34; the core is only constrained by two ages, whereas core 012P is constrained by eight. Therefore, based on the high similitude of the two units and the weaker age model of core 34, we interpret the lowermost units of both cores to be of similar glacial origin.

Similarly, sub-unit 1b) (Fig. 7a), from 10500 to 9300 a cal BP, resembles intervals 12-4 and 12-5 of core 012P, which are dated from 11300 to 9500 a cal BP (Knudsen *et al.*, 2008). At this time, the sedimentary environment was influenced by the WGC and by the surrounding permanent to semi-permanent sea-ice cover (Knudsen *et al.*, 2008; Jennings *et al.*, 2011). The presence of pebbles in the sediment is also an indicator of extensive sea-ice cover or icebergs according to Knudsen *et al.* (2008). On the other hand, traces of bioturbation are visible on sub-unit 1b) but apparently not in the corresponding intervals in core 012P (Knudsen *et al.*, 2008). The southernmost position of core 34 may provide an explanation of the presence of bioturbation, as the site was probably more affected by the warm WGC instead of permanent sea-ice cover.

This interpretation, i.e. a diamictite followed by meltwater deposits and ice rafted debris, is coherent with the other properties of core 34. The presence of a more pronounced red color (a^*) associated with lower magnetic remanence values (NRM, ARM and IRM) could reflect the presence of hematite that was transported by glaciers from the Thule Basin (Dawes, 2006). The presence of small pebbles around 10 000 a cal BP is also highlighted by peaks in the magnetic properties (k_{LF} , NRM, ARM and IRM).

Unit 2, from 9350 a cal BP to present, is an alternation of sub-units with the presence or absence of traces of bioturbation (Fig. 7a). This unit is in accordance with the facies E observed by Aksu and Piper (1987) in Baffin Bay, i.e. greenish-gray fine muds interpreted as hemipelagic sediments. Sub-unit 2d), from 2500 a cal BP to present, shows a slight increase in mean grain size. Coarser sediment can indicate an increase in bottom current velocity. The augmentation in mean grain size is also observed at the top core 012P from 2500 a cal BP to present, particularly between 800 to 200 a cal BP (Knudsen *et al.*, 2008). In combination with foraminifera and diatom assemblages, the authors interpreted this

interval by an incursion of cold CO₂-rich Arctic bottom waters (Knudsen *et al.*, 2008; Jennings, 1993). Moreover, the presence of cold CO₂-rich waters increases the carbonate dissolution process (Stein, 2008). Because the L* values can often be an indicator of the carbonate content (Ortiz *et al.*, 1999; Simon *et al.*, in press), the decrease observed starting at 700 cal a BP (Fig. 7a) also supports this interpretation. Once again, based on the similarities of both units, we interpret them as a common signal.

Site 38 – North Water Polynya

The coring site of core 38 is very close (78 km directly to the South) of core 008P of Knudsen *et al.* (2008). Both cores are composed of homogeneous and highly bioturbated olive-grey to dark-olive grey siltly clays. According to Knudsen *et al.* (2008), sedimentation occurred mainly by suspension. Unit 1 of core 38, from 8660 to 5650 a cal BP, is very rich in shell fragments and has numerous sinuous millimeter-scale burrows (Fig. 7b). From the top to the base of unit 1, there is a slight increase in density values associated with downcore compaction. This unit also shares similarities with a 112-cm layer of highly bioturbated mud described by Jennings *et al.* (2011) from core HLY03-05GC from Hall Basin in Nares Strait. This 8930 to 160 a cal BP interval corresponds to the Nares Strait post opening period. According to Jennings *et al.* (2011), based on pervasive bioturbation, as well as the benthic and planktonic foraminifera assemblages, there is indication of a high marine productivity between 8926 to 6050 a cal BP. This is followed by a decline in productivity indicators and cooler conditions during the Neoglacial period.

For unit 1 of core 38, the very high degree of bioturbation, shells and shell fragments are an indication of high productivity. In addition, the base of core 38 is dated at 8660 a cal BP. This is more than 300 years after the opening of Nares Strait (Jennings *et al.*, 2011), most likely explaining the absence of ice-contact sediments or IRD in the unit.

At the very bottom of the unit, there is a progressive decrease of NRM, ARM and IRM values (Fig. 7b). This decrease can be related to a change in sediment source. Sediments

from meltwaters are rich in ferrimagnetic grains, which originate from the Precambrian granitic complex surrounding Baffin Bay (Andrews and Jennings, 1990; Aksu and Piper, 1987). In contrast, deposition of hemipelagic sediment when the WGC is dominant is associated with low magnetic susceptibility as seen in this study.

Unit 2, from 5650 a cal BP to top of the core, is very homogeneous (Fig. 7b). All the properties are similar to those of unit 2 of core 34, with lower magnetic property values. Sub unit-2b), from 3700 to 2200 a cal BP, is characterized by higher values in density, k_{LF} , NRM, ARM and IRM, which are explained by pebbles and coarser magnetic grain sizes (Fig. 7B). A major peak in k_{LF} , at 3300 a cal BP, is directly caused by the presence of pebbles which likely indicate deposition by IRD. Wanner *et al.* (2011) identified six cold events during the Holocene in the Northern Hemisphere. They determined a cold event between 3300 and 2500 a cal BP corresponding to an ice rafted debris event reported in the North Atlantic by Bond *et al.* (1997). This event was notably associated with a deep Iceland Scotland Overflow Water (ISOW) minimum (Hall *et al.*, 2004). A peak in sea-ice diatoms, at 2730 a cal BP, was also observed by Knudsen *et al.* (2008), and is associated with a cool and unstable environment for the interval of 3050 to 2550 a cal BP. During that interval, Andresen *et al.* (2010) also reported an episode of iceberg calving in Disko Bugt. So, we interpret this presence of pebbles as ice rafted debris generated by icebergs at the mouth of Nares Strait during this cold event.

Site 42 – Jones Sound

The lowermost unit of core 42, from 10650 to 8350 a cal BP, is composed of rock fragments, pebbles, turbidites and sand laminations in a compact reddish silty clay matrix (Fig. 7c). A similar layer is observed in Ledu *et al.* (2010) at the base of core 2004-804-009PC in Lancaster Sound, which is located between Devon and Baffin Island. Ledu *et al.* (2010) described it as brown sand with grayish brown silty clay layers deposited between 11100 to 10800 a cal BP and associated it with large terrigenous inputs from the final collapse of the Innuitian Ice Sheet (IIS) in the Canadian Arctic Archipelago. Similarly, we interpret this layer as being associated with deglaciation in the early Holocene.

Indeed, Sub-unit 1a), from 10650 to 10250 a cal BP, with its large and numerous pebbles is similar to unit 1 of core 34 and is also interpreted as a diamictite (Fig. 7c). According to England *et al.* (2006), break-up of the IIS in the Queen Elizabeth Island region, including Ellesmere Island and Jones Sound, started around 11100 a cal BP. Then, the ice retreated to leave progressively more room for marine embayment until 9000 a cal BP. Sub-unit 1b), from 10250 to 8350 a cal BP, is interpreted as a mixture of IRD and turbidites caused by meltwaters and icebergs from the melting of the ISS on Devon and Ellesmere Islands (England *et al.*, 2006).

Unit 2, from 8350 to 550 a cal BP, is visually very homogeneous, but sub-units were determined by changes in MDF and $\text{ARM}_{20\text{mT}}/\text{ARM}_{0\text{mT}}$ (Fig. 7c). Sub-unit 2a) presents higher MDF values, which can be explained by a finer magnetic grain size. The chronology of this sub-unit, from 8350 to 5250 a cal BP is concurrent with the Holocene Climatic Optimum for the region (Ledu *et al.*, 2010; Jennings *et al.*, 2011; Koç and Jansen, 2002).

Moreover, the MDF profile of the whole core is almost identical to the variations of key paleoceanographic proxies of core HLY03-05GC (Jennings *et al.*, 2011) from Nares Strait (Fig. 8). The relationship between the $\delta^{18}\text{O}$ and $\delta^{13}\text{C}$ records and the median destructive field is not exactly determined, but in the past, some links have been established between the dilution of terrigenous material with biogenic sediments and changes in magnetic mineralogy (Brachfeld and Banerjee, 2000; Brachfeld, 2006). In this case, the link between MDF, $\delta^{18}\text{O}$ and $\delta^{13}\text{C}$ records probably occurs due to the influence of meltwaters and the proximity of ice. The meltwater episode before the opening of Nares Strait is associated with warmer surface conditions ($\delta^{18}\text{O}$), low marine productivity ($\delta^{13}\text{C}$) (Jennings *et al.*, 2011) and coarser terrigenous material (lower MDF). The Holocene climatic optimum is then characterized by the occurrence of finer sediment due to hemipelagic sedimentation, which results in higher MDF values and high marine productivity ($\delta^{13}\text{C}$). Finally, the Neoglacial period is characterized by an increase in sea ice cover ($\delta^{18}\text{O}$) and a decrease in marine productivity ($\delta^{13}\text{C}$) (Jennings *et al.*, 2011), as well as an increase in coarser ice-

transported sediment that gives lower MDF values. This is coherent with a constant pseudo S ratio for the period following the deglaciation (i.e. from 8375 to 1750 a cal BP) (Fig. 5c) which also means a constant mineralogy. But for the top of the core, where an increase in MDF, a small increase in the pseudo S ratio and remanence (NRM, ARM and IRM) values have no corresponding $\delta^{18}\text{O}$ and $\delta^{13}\text{C}$ change, the variation is associated to an increase in the concentration of low coercivity minerals such as magnetite.

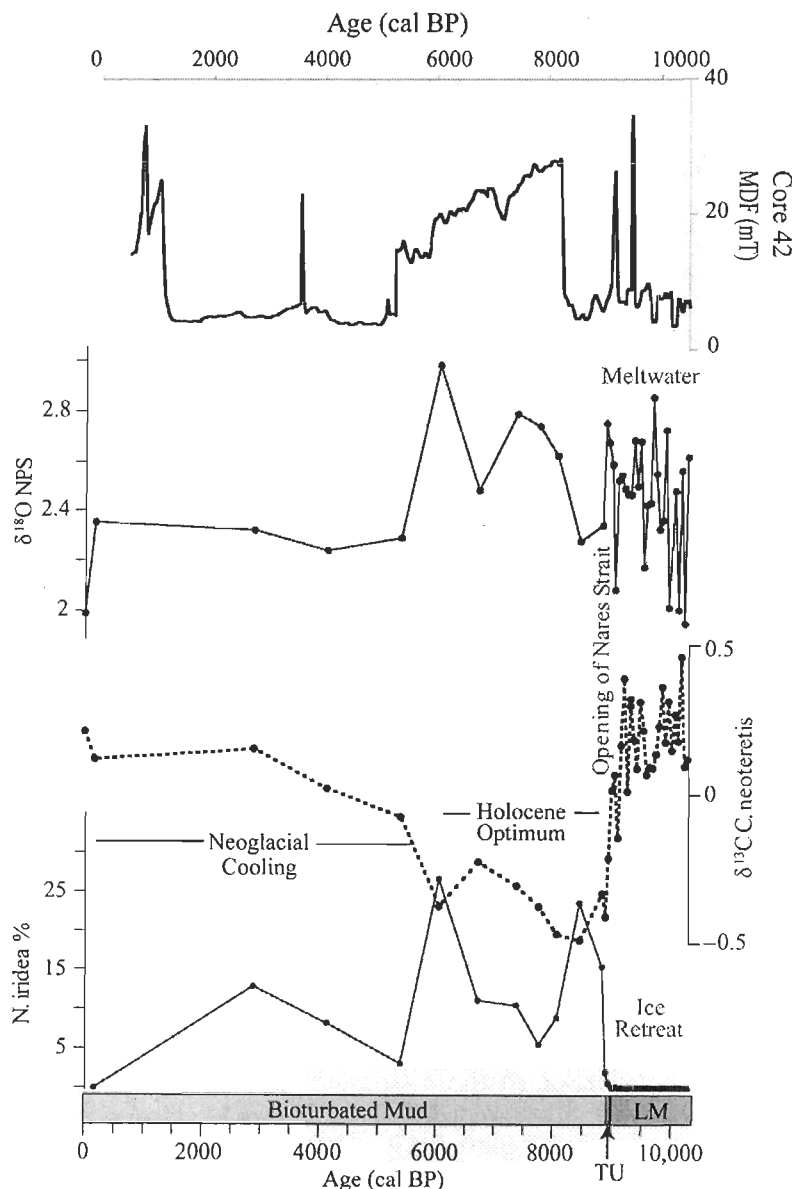


Figure 6. Comparison between the MDF profile of core 42 and key paleoceanographic proxies of core HLY03-05GC from Jennings *et al.* (2011). TU is for the transitional unit associated to the opening of Nares Strait observed in core HLY03-05GC. LM is for the Last Glacial Maximum.

Core 70 – Disko Bugt

Core 70 covers sediment changes from 12275 to 420 a cal BP (Fig. 7d). Figure 9 illustrates the comparison between density and k_{LF} profiles and two temperature profiles from the Greenland Ice Core Project (GRIP) borehole (Dahl-Jensen *et al.*, 1998), as well as a compilation from ice-core records in Greenland (Weidick and Bennike, 2007). Overall, the curves are similar and suggest that the density and k_{LF} profiles are good indicators of climate changes in Disko Bugt for this period.

Unit one, from 12275 to 11230 a cal BP, is composed of many pebbles and shell fragments in a sandy mud matrix (Fig. 7d). This period corresponds to the presence of the Jakobshavn Isbrae ice stream near the Inner Egedesminde Dyb (channel), 165 km to the east of the sampling site of core 70. The transition from the Younger Dryas to the Holocene (12600 - 11700 a cal BP) was likely characterized by a significant influx of meltwaters (Weidick and Bennike, 2007), while the presence of pebbles in core 70 indicates the passage of icebergs (Stein, 2008). This unit is thus interpreted to reflect meltwater inputs and IRD deposition during the beginning of deglaciation in Disko Bugt.

Unit two, from 11230 to 7410 a cal BP, corresponds to the transition from the deglaciation and the Holocene Thermal Optimum (Fig. 7d). According to Weidick and Bennike (2007), the Jakobshavn Isbrae glacier reached its current position around 6000-7000 a BP (see Figure 9). Unit 2a), from 11230 to 9475 a cal BP, still contains pebbles but in a finer matrix. This indicates an increase in the distance between site 70 and the meltwater source. Unit 2b), from 9475 to 7410 a cal BP, contains traces of bioturbation. It is concomitant with the establishment of the WGC in the bay, between 9200 and 7800 a cal BP (Lloyd *et al.*, 2005). The transition in the sediment origin, from glacial meltwaters to WGC hemipelagic deposition, is observable in the age model of core 70 (Fig. 6) with a major change in sedimentation rates at ~8800 a cal BP, passing from 75 cm/ka to 20 cm/ka.

Unit three, from 7410 to 420 a cal BP, is homogeneous, slightly bioturbated and contains a 10-cm turbidite at ~1885 a cal BP (Fig. 7d). This turbidite could have been deposited

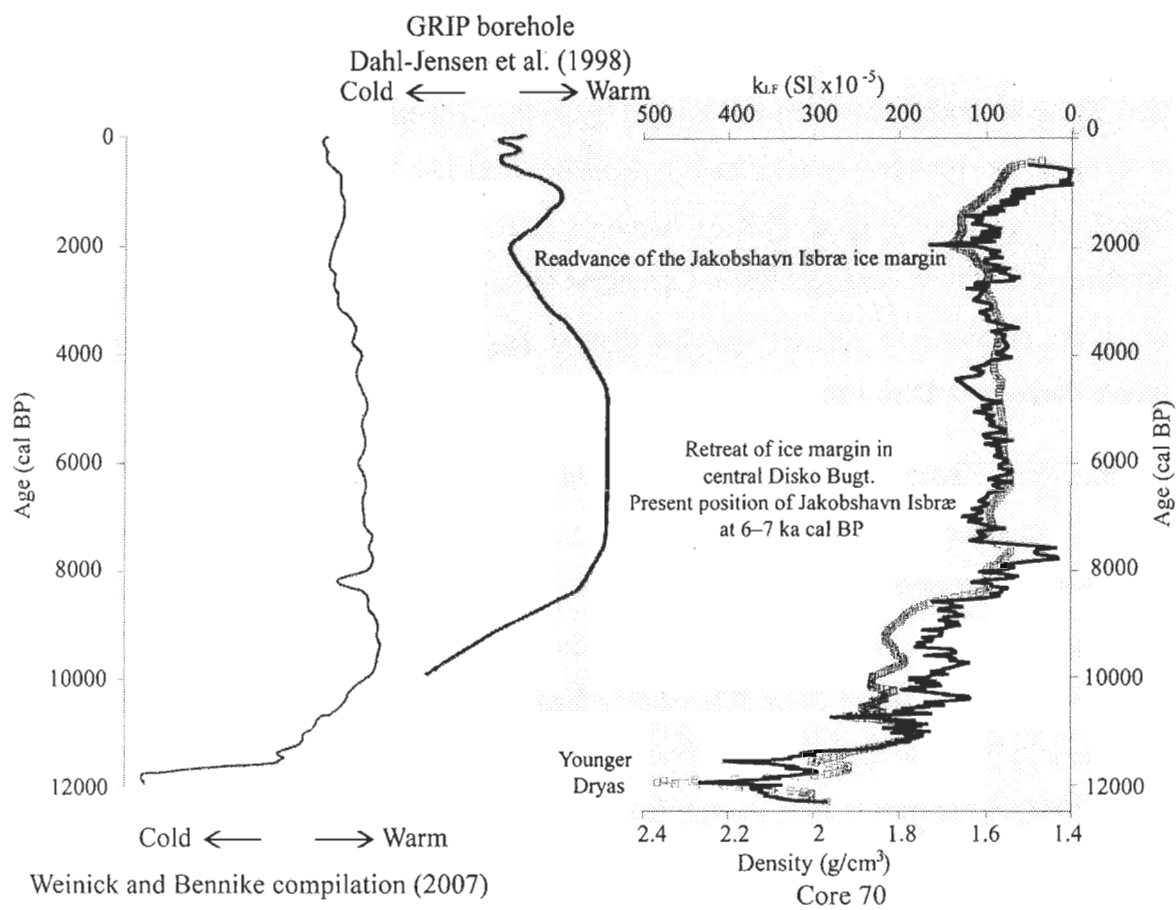


Figure 7. Comparison of the magnetic susceptibility (blue squares) and density (black line) profiles of core 70 with temperature profiles from Weinick and Bennike (2007) and Dahl-Jensen *et al.* (1998) (ice core).

following an intense episode of iceberg rafting. Indeed, four episodes of short-lived iceberg rafting have been identified by Andresen *et al.* (2010) in Disko Bugt at 5000, 3700, 2300 and 2100 a cal BP. The turbidite observed at ~1885 a cal BP could be the result of the most recent ice rafting event. This event could be the result of a period of warmer WGC (Lloyd *et al.*, 2005; Andresen *et al.*, 2010) that would have caused an increase in meltwater outflow and iceberg calving (Moros *et al.*, 2006, Andresen *et al.*, 2010).

According to Weidick and Bennike (2007), the climatic optimum in Disko Bugt was recorded from 8 to 5-4 ka cal BP. The increase in sea surface temperatures for the southeastern part of Baffin Bay during the thermal maximum is caused by the influence of the WGC over the meltwater from the Jakobshavn Isbrae ice stream and local glaciers from Disko Island (Kelly and Lowell, 2009; Lloyd *et al.*, 2005). This period is associated with unit 3 of core 70, which is characterized by homogeneous and slightly bioturbated hemipelagic sediments. Finally, there is no unit associated with the Neoglacial period observed in Northern Baffin Bay, from 4000 a cal BP to present (Jennings *et al.*, 2011) in core 70.

Paleomagnetic secular variations in the Eastern and Western Canadian Arctic

Figures 10 and 11 illustrate a comparison between the directional variations of the three most reliable cores from this study, and others from the Eastern (Baffin bay inclination stack - Andrews and Jennings, 1990) and Western Canadian Arctic (Chukchi Sea: core HLY0501-08JPC- Lisé-Pronovost *et al.*, 2009; core HLY0501-05JPC - Barletta *et al.*, 2008). These three cores were selected in order to compare geomagnetic field behaviour in the Eastern and Western Canadian Arctic. When compared together, the inclination (Fig. 10) and declination records (Fig. 11) of cores 34, 42 and 70 show a general agreement at the millennial timescale. Moreover, the millennial-scale directional features are also coherent with the records from the Chukchi Sea and with the Baffin Bay inclination stack. In addition, from the base of all the records to about 6000 a cal BP, declination values are

increasing. Some of the differences in the timing of the individual directional features are probably the result of the different chronologies, sedimentation rates or lock-in depths.

These comparisons allow us to assert that most of the secular to millennial-scale geomagnetic variations are observed from the Eastern to the Western Canadian Arctic and are coherent with other North American paleomagnetic records, indicating a similar behavior at the scale of the Canadian Arctic. The coherence between these results and others from mid-latitudes of North America (St-Onge and Stoner, 2011) suggests that even the northernmost record from Smith Sound at 76°N has a behavior typical of the rest of North America which does not seem to be accentuated by the coring site being located within the tangent cylinder. A similar conclusion was drawn by Sagnotti *et al.* (2011) regarding the paleomagnetic records from the Barents Sea at latitudes of 75°–76° N. At the scale of North America, the similarities of the paleomagnetic records from the Western and Eastern Canadian Arctic have important chronostratigraphic implications as cores from the Arctic are often challenging to date because of calcium carbonate dissolution and the often poorly constrained radiocarbon reservoir effect. Indeed, knowing that the paleomagnetic secular variations are coherent from the Western and Eastern Canadian Arctic to at least 76°N suggests that the paleomagnetic data from well-dated reference cores can be used to correlate and improve the chronology of problematic Canadian Arctic cores.

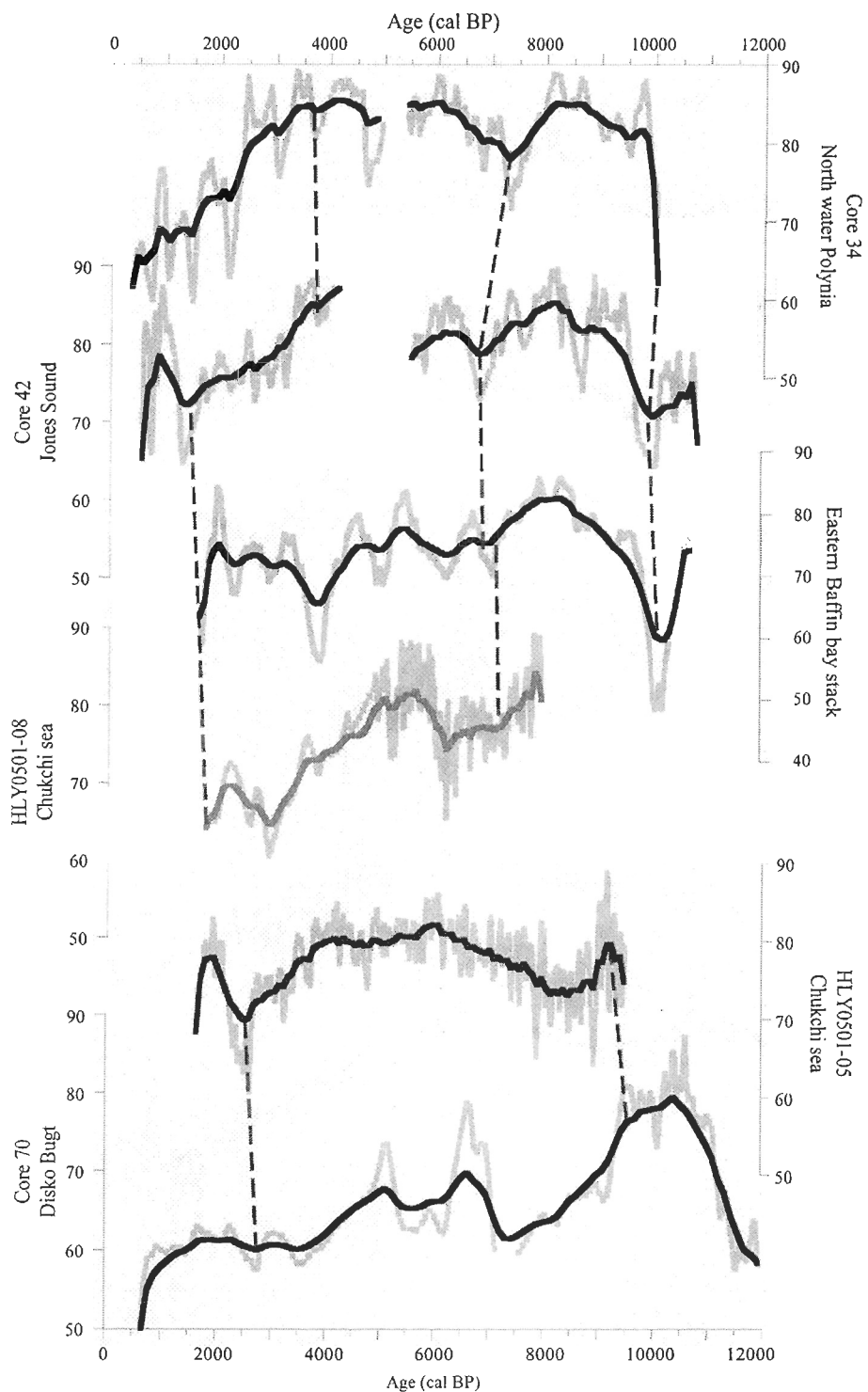


Figure 8. Comparison of inclination profiles between cores 34, 42 and 70 (this study) with cores from the eastern Canadian Arctic (Eastern Baffin bay stack; Andrews and Jennings, 1990) and western Canadian Arctic (HLY0501-08JPC; Lisé-Pronovost *et al.*, 2009, HLY0501-05; Barletta *et al.*, 2008). The original age scale of the Eastern Baffin Island stack from Andrews and Jennings (1990) was converted to calibrated ages.

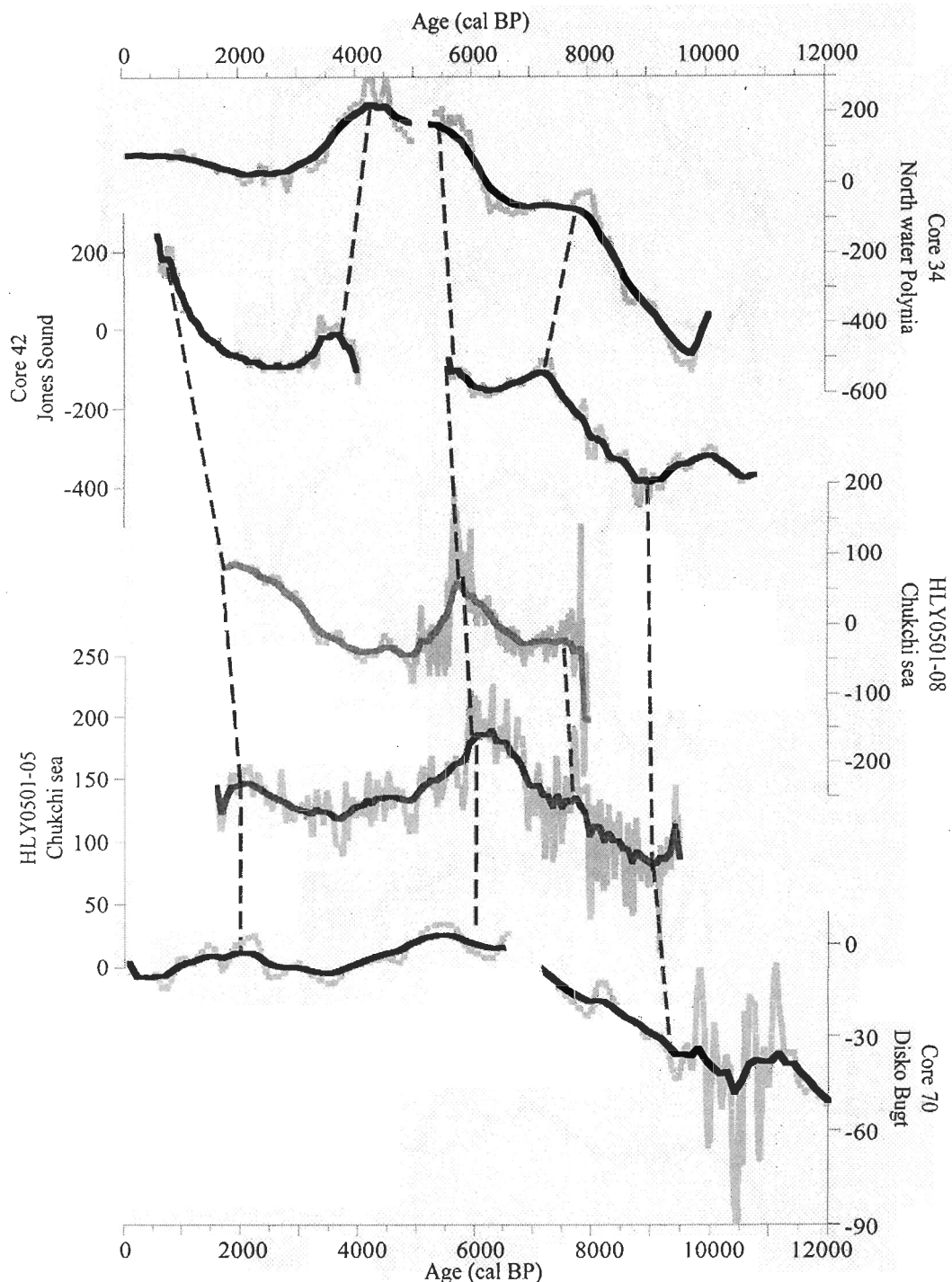


Figure 9. Comparison of the declination profiles between cores 34, 42 and 70 (this study) with cores from the western Canadian Arctic (HLY0501-08JPC; Lisé-Pronovost et al., 2009, HLY0501-05JPC; Barletta et al., 2008).

Conclusions

The main lithofacies of the four cores reflect major Holocene environmental changes (Jennings *et al.*, 2011; Wanner *et al.*, 2011, Knudsen *et al.*, 2008; Weidick and Bennike, 2007). Cores 34, 42 and 70 recorded the transition between the Younger Dryas and the Holocene. All the cores have a homogeneous signal for the Holocene climatic optimum. On the other hand, the Neoglacial period signature, when present, is only local. Indeed, core 38 has a specific signal of IRD and coarse grains for the cold event of 2500-3300 a cal BP (Wanner *et al.*, 2011) and core 70 contains a turbidite dated at ~1885 a cal BP and associated with a local iceberg production generated by an episode of warmer WGC (Moros *et al.*, 2006, Andresen *et al.*, 2010).

Regarding the paleomagnetic signal, the new results illustrate that for three of the four cores, directional data are of very good quality for recording the changes in Earth's magnetic field direction during the Holocene. When we compare these results to others from the Canadian Arctic, similar millennial-scale features are observed, indicating that the geomagnetic field behaviour is similar up to at least 76°N in the low western and eastern Canadian Arctic. These results suggest the reliability of well-dated reference cores as a chronostratigraphic tool in the low Arctic.

Acknowledgements

We are grateful to the captain, officers, crew and scientists on board of the CCGS *Hudson* during the 2008-029 expedition funded by the Geological Survey of Canada and the Natural Sciences and Engineering Research Council of Canada (NSERC). This study was supported by the *Fonds Québécois de recherche en Nature et Technologies*, NSERC and by the Economic Development, Innovation and Export Trade Ministry of Quebec (Canadian

contribution to the Past4Future project). We sincerely thank Anne Jennings (INSTAAR) for sharing the ^{14}C dates of core 70 and for commenting the preliminary version of this paper. We also thank Joseph Ortiz (Kent State University) for the diffuse spectral reflectance measurements. Finally, we thank David Ledu (LOCEAN) for calibrating the radiocarbon ages of the Baffin Bay inclination stack of Andrews and Jennings (1990).

References

- Aksu, A. 1981. Late Quaternary Stratigraphy, Palaeoenvironmentology and Sedimentation History of Baffin Bay and Davis Strait. Ph.D. dissertation, Dalhousie University, 771 pages.
- Aksu AE, Piper DJW. 1987. Late Quaternary sedimentation in Baffin Bay. *Canadian Journal of Earth Science* **24**: 1833-1846.
- Andersen, OGN. 1981. The annual cycle of temperature, currents and water masses in Disko Bugt and adjacent waters. West Greenland. Meddelelser om Grønland. Bioscience 5, 1–36.
- Andresen C, David JS, McCarthy C *et al.* 2010. Interaction between subsurface ocean waters and calving of the Jakobshavn Isbræ during the late Holocene. *The Holocene* **21**: 221–224.
- Andrews JT, Jennings AE. 1990. Geomagnetic secular variations (inclination) of high latitude fiord cores: eastern Canadian Arctic. *Polar Research* **8** : 245-259.
- Andrews JT, Hardadottir J, Stoner JS. 2003. Decadal to millennial-scale periodicities in North Iceland shelf sediments over the last 12 000 cal yr: long-term North Atlantic oceanographic variability and solar forcing. *Earth and Planetary Science Letters* **210** : 453-465.

- Antoniades D, Francus, Pienitz R, St-Onge G, Vincent WF. 2011. Holocene dynamics of the Arctic's largest ice shelf. *Proceedings of the National Academy of Sciences* **108** : 18899–18904.
- Barber D, Marsden R, Minnett P *et al.* 2001. Physical processes within the North Water (NOW) polynya. *Atmosphere-Ocean* **39** : 163-166.
- Barletta F, St-Onge G, Channell JET, Rochon A, Polyak L, Darby D. 2008. High-resolution paleomagnetic secular variation and relative paleointensity records from the western Canadian Arctic: implication for Holocene stratigraphy and geomagnetic field behavior. *Canadian Journal of Earth Sciences* **45**: 1265-1281.
- Barletta F, St-Onge G, Channell JET, Rochon A. 2010. Dating of Holocene Western Canadian Arctic sediments by matching paleomagnetic secular variation to a geomagnetic field model. *Quaternary Science Reviews* **29** : 2315-2324.
- Blott SJ, Pye K. 2001. Gradistat: a grain size distribution and statistics package for the analysis of unconsolidated sediments. *Earth Surface Processes and Landforms* **26** : 1237–1248.
- Bond, G, Showers, W, Cheseby, M, *et al.* 1997. A pervasive millennial-scale cycle in the North Atlantic Holocene and glacial climates. *Science* **294** : 2130-2136.
- Brachfeld SA, Banerjee SK. 2000. Rock-magnetic carriers of century-scale susceptibility cycles in glacial^marine sediments from the Palmer Deep, Antarctic Peninsula. *Earth and Planetary Science Letters* **176**: 443-455.
- Brachfeld SA. 2006. High-field magnetic susceptibility (χ_{HF}) as a proxy of biogenic sedimentation along the Antarctic Peninsula. *Physics of the Earth and Planetary Interiors* **156** : 274-282.
- Dahl-Jensen D, Mosegaard K, Gundestrup N, *et al.* 1998. Past Temperatures Directly from the Greenland Ice Sheet. *Science* **282** : 268-271.

- Dankers, P. 1981. Relationship between median destructive field and remanent coercive forces for dispersed natural magnetite, titanomagnetite and hematite. *Geophysical Journal of the Royal Astronomical Society* **64** : 447–461.
- Day R, Fuller M, Schmidt VA. 1977. Hysteresis properties of titano-magnetite: grain- size and compositional dependence. *Physics of the Earth and Planetary Interiors* **13** : 260–267.
- de Vernal A, Rochon A. 2011. Dinocysts as tracers of sea-surface conditions and sea-ice cover in polar and subpolar environments. *IOP Conference Series: Earth and Environmental Science* **14** : 012007.
- Dawes PR. 2006. Explanatory notes to the Geological map of Greenland, 1:500 000, Thule, Sheet 5. *Geological Survey of Denmark and Greenland, Map Series 2*.
- Dearing J. 1999. *Environmental Magnetic Susceptibility: Using the Bartington MS2 System*. Chi Publishing Kenilworth, UK.
- Dowdeswell JA, Elverhøi A, Spielhagen R. 1998. Glacimarine sedimentary processes and facies on the Polar North Atlantic margins. *Quaternary Science Reviews* **17** : 243–272.
- England JH, Atkinson N, Bednarski JB, et al. 2006. The Innuitian Ice Sheet: Configuration, dynamics and chronology. *Quaternary Science Reviews* **25**:689–703.
- Hall IR, Bianchi GG, Evans JR. 2004. Centennial to millennial scale Holocene climate-deep water linkage in the North Atlantic. *Quaternary Science Reviews* **23** : 1529–1536.
- Hogan KA, Dix JK, Lloyd JM, et al. 2011. Seismic stratigraphy records the deglacial history of Jakobshavn Isbræ, West Greenland. *Journal of Quaternary Science* **26** : 757-766.

- Hogan KA, Dowdeswell JA, Cofaigh CO. 2012. Glacimarine sedimentary processes and depositional environments in an embayment fed by West Greenland ice streams, *Marine Geology* **311** : 1-16.
- Holland MM, Bitz CM, Eby M, *et al.* 2001. The Role of Ice–Ocean Interactions in the Variability of the North Atlantic Thermohaline Circulation. *Journal of Climate* **14**: 656–675.
- Hughen, KA, Baillie MGL, Bard E, *et al.* 2004. Marine04 Marine radiocarbon age calibration, 26 - 0 ka BP. *Radiocarbon* **46**, 1059-1086.
- Jennings AE. 1993. The Quaternary History of Cumberland Sound, Southeastern Baffin Island: The Marine Evidence. *Géographie physique et Quaternaire* **47**: 21-42.
- Jennings AE, Walton ME. 2010. Reconstruction of Early Holocene West Greenland Ice Sheet and West Greenland Current Using Radiocarbon Dating and Foraminiferal Assemblages. *The State of the Arctic Conference*, Miami, Florida, USA. Poster.
- Jennings AE, Sheldon C, Cronin TM, *et al.* 2011. The Holocene history of Nares Strait: Transition from glacial bay to Arctic-Atlantic throughflow. *Oceanography* **24** : 26–41.
- Jennings AE, Walton ME, O’Cofaigh C, Kilfeather A, Andrews, JT, Ortiz, DeVernal, A, Dowdeswell JD. Paleoenvironments during Younger Dryas-Early Holocene Greenland Ice Sheet retreat from outer Disko Trough, central west Greenland. *Journal of Quaternary Science*, this issue.
- Johnsen SJ, Dahl-Jensen D, Gundestrup N. *et al.* 2001. Oxygen isotope and palaeotemperature records from six Greenland ice-core stations: Camp Century, Dye-3, GRIP, GISP2, Renland and NorthGRIP. *Journal of Quaternary Science* **16** : 299–307.

- Kelly MA, Lowell TV. 2009. Fluctuations of local glaciers in Greenland during latest Pleistocene and Holocene time. *Quaternary Science Reviews* **28**: 2088–2106.
- Kirschvink, JL. 1980. The least-squares line and plane and the analysis of paleomagnetic data. *Geophysical Journal of the Royal Astronomical Society* **62** : 699-718.
- Knudsen KL, Stabell B, Seidenkrantz MS, *et al.* 2008. Deglacial and Holocene conditions in northernmost Baffin Bay: sediments, foraminifera, diatoms and stable isotopes. *Boreas* **37** : 346-376.
- Koç N, Jansen E. 2002. Holocene Climate Evolution of the North Atlantic Ocean and the Nordic Seas- A Synthesis of New Results, 165-173. In *Climate development and history of the North Atlantic realm*, Wefer G, Berger WH, Behre KE, Jansen E (eds). Springer : Berlin Heidelberg New York ; 486 pages.
- Korte M, Constable C, Donadini F, *et al.* 2011. Reconstructing the Holocene geomagnetic field. *Earth and Planetary Science Letters* **312**: 497-505.
- Krawczyk D, Witkowski A, Moros M, *et al.* 2010, Late-Holocene diatom-inferred reconstruction of temperature variations of the West Greenland Current from DiskoBugt, central West Greenland. *The Holocene* **20** : 659–666.
- Ledu D, Rochon A, de Vernal A, *et al.* 2010. Holocene paleoceanography of the Northwest Passage, Canadian Arctic Archipelago. *Quaternary Science Reviews* **29**: 3468-3488.
- Levac E, de Vernal A, Blake WJ. 2001. Sea-surface conditions in northernmost Baffin Bay during the Holocene: palynological evidence. *Journal of Quaternary Science* **16** : 353–363.
- Lisé-Pronovost A, St-Onge G., Brachfeld S, *et al.* 2009. Paleomagnetic constraints on the Holocene stratigraphy of the Arctic Alaskan margin. *Global and Planetary Change* **68** : 85-99.

- Lloyd JM, Parka LA, Kuijpers A, *et al.* 2005. Early Holocene palaeoceanography and deglacial chronology of Disko Bugt, West Greenland. *Quaternary Science Reviews* **24** : 1741–1755.
- Lloyd JM. 2006. Late Holocene environmental change in Disko Bugt, west Greenland: interaction between climate, ocean circulation and Jakobshavn Isbrae, *Boreas* **35** : 35–49.
- Lloyd JM, Kuijpers A, Long A, *et al.* 2007. Foraminiferal reconstruction of mid- to late-Holocene ocean circulation and climate variability in Disko Bugt, West Greenland. *The Holocene* **17** : 1079–1091.
- Mazaud A. 2005. User-friendly software for vector analysis of the magnetization of long sediment cores. *Geochemistry Geophysics Geosystems* **6** : Q12006.
- Melling H, Gratton Y, Ingram G. 2001. Ocean circulation within the North Water polynya of Baffin Bay. *Atmosphere-Ocean* **39**: 301–325.
- Miller GH, Wolfe AP, Briner JP, *et al.* 2005. Holocene glaciations and climate evolution of Baffin Island, Arctic Canada. *Quaternary Science Review* **24**: 1703–1721.
- Moros M, Jensen KG and Kuijpers A. 2006. Mid- to late-Holocene variability in Disko Bugt, central West Greenland. *The Holocene* **16**: 357–367.
- Ólafsdóttir S, Geirsdóttir Á, Miller GH, Stoner JS, Channell JET, in press. Synchronizing Holocene Lacustrine and Marine Sediment Records in Iceland Using Paleomagnetic Secular Variation. Submitted to: *Geology*.
- Ortiz JD, Mix A, Harris S, *et al.* 1999. Diffuse spectral reflectance as a proxy for percent carbonate content in North Atlantic sediments. *Paleoceanography* **14** : 171–186.

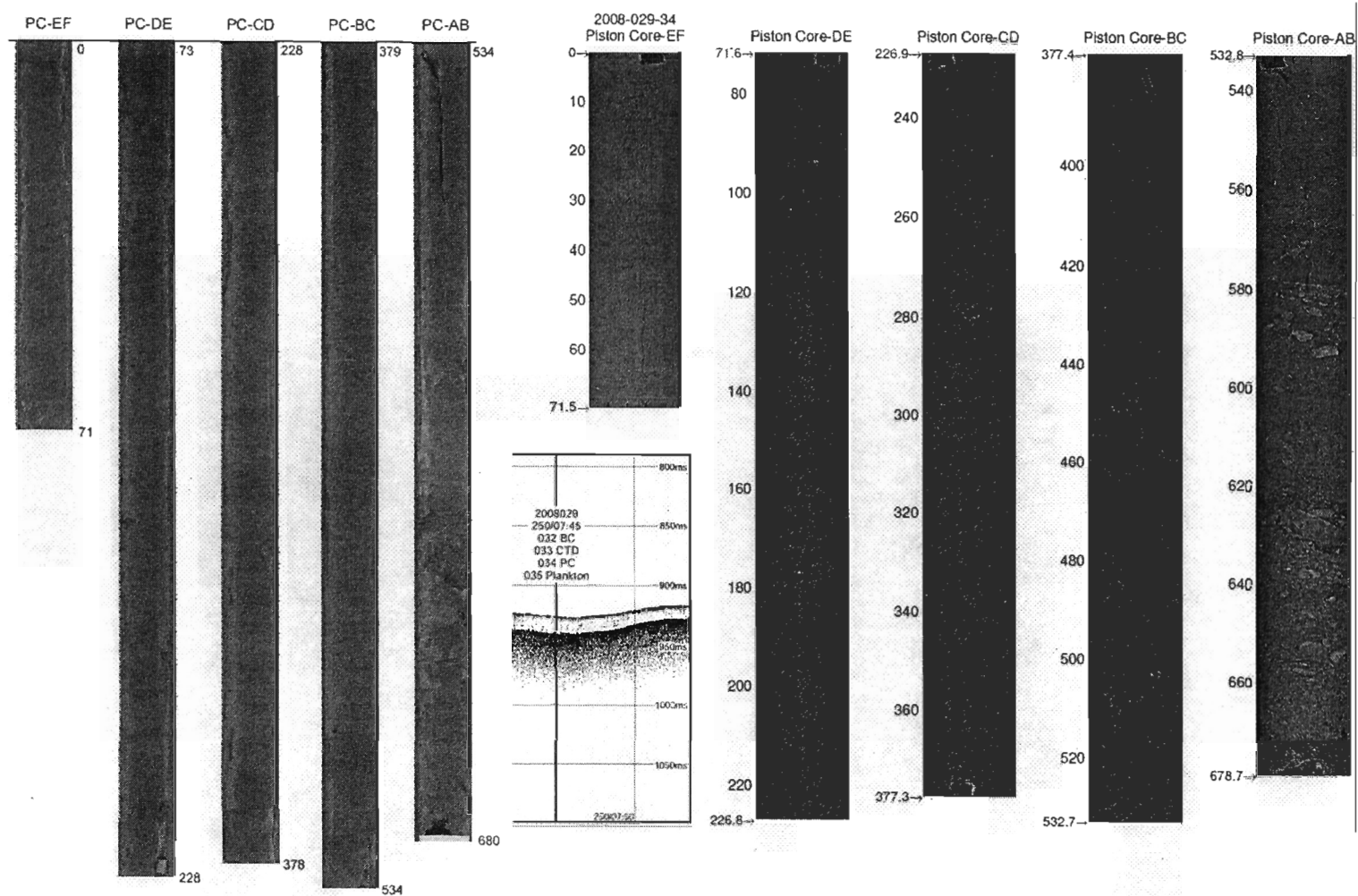
- Perner K, Moros M, Lloyd JM, *et al.* 2011. Centennial scale benthic foraminiferal record of late Holocene oceanographic variability in Disko Bugt, West Greenland. *Quaternary Science Reviews* **30** : 2815-2826.
- Ribergaard MH, Olsen SM and Mortensen J. 2008. Oceanographic Investigations off West Greenland 2007, NAFO SCR Doc. 08/3, SCIENTIFIC COUNCIL MEETING – JUNE 2008
- Roberts N. 2002. *The Holocene, an environmental history*. Second edition. Blackwell publishers.
- Roberts AP. 2006. High-resolution magnetic analysis of sediment cores: Strengths, limitations and strategies for maximizing the value of long-core magnetic data. *Physics of the Earth and Planetary Interiors* **156** :162-178.
- Sagnotti L, Macrì P, Lucchi R, *et al.* 2011. A Holocene paleosecular variation record from the northwestern Barents Sea continental margin. *Geochemistry, Geophysics, Geosystems* **12** : Q11Z33.
- Seppä H, Cwynar LC MacDonald GM. 2003. Post-glacial vegetation reconstruction and a possible 8200 cal. yr BP event from the low arctic of continental Nunavut, Canada. *Journal of Quaternary Science* **18** : 621–629.
- Simon Q, St-Onge G, Hillaire-Marcel C. 2012. Late Quaternary chronostratigraphic framework of deep Baffin Bay glaciomarine sediments from high-resolution paleomagnetic data. *Geochemistry Geophysics Geosystems* **13**: in press.
- Stein R. 2008. *Arctic Ocean Sediments: Processes, Proxies, and Palaeoenvironment*. Developments in Marine Geology, Vol. 2, Elsevier : Amsterdam.
- Stoner JS, Channell JET, Hillaire-Marcel C. 1996. The magnetic signature of rapidly deposited detrital layers from the deep Labrador Sea: relationship to North Atlantic Heinrich layers. *Paleoceanography* **11** : 309-325.

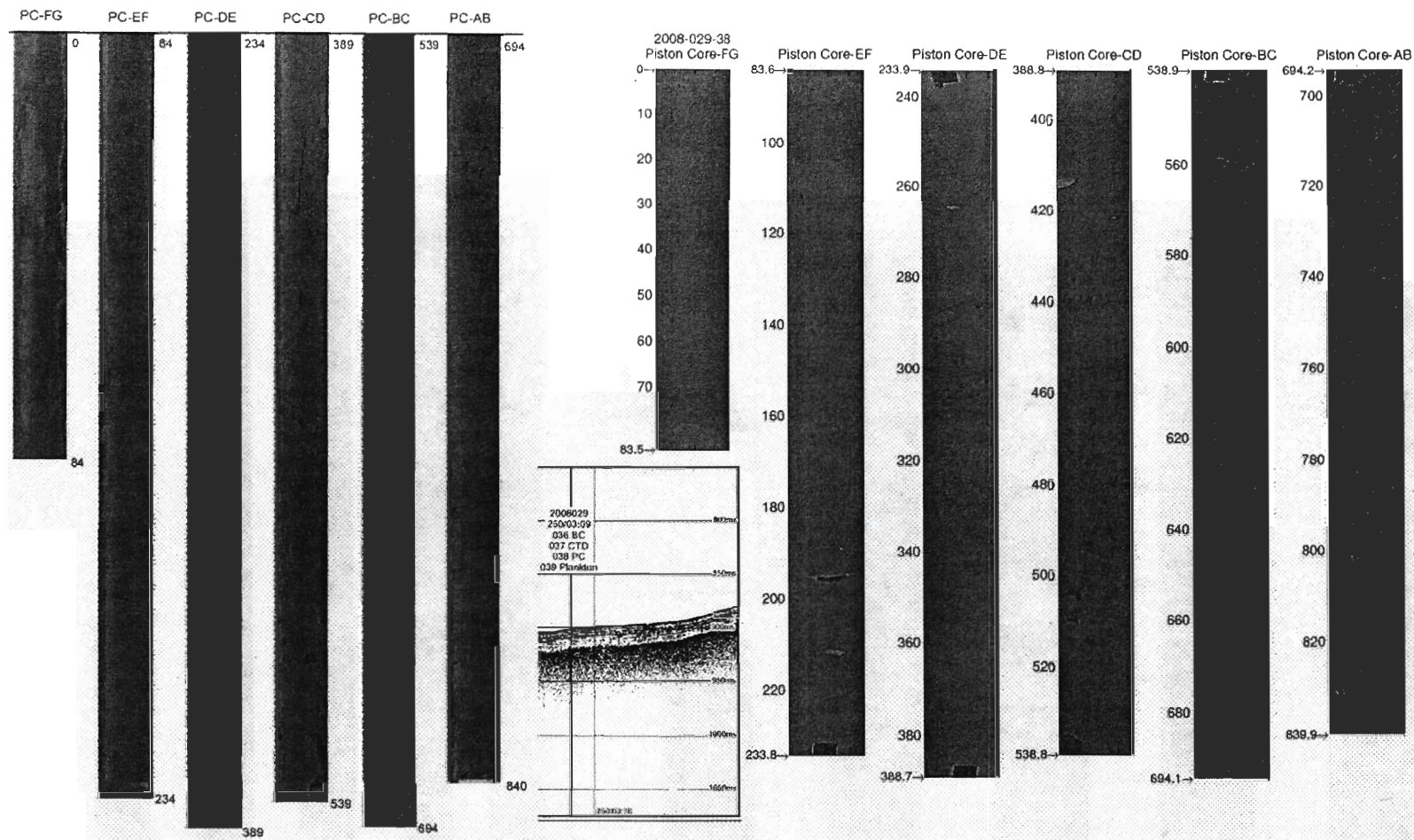
- Stoner JS, St-Onge G. 2007. Magnetic Stratigraphy in Paleoceanography: Reversals, Excursions, Paleointensity, and Secular Variation in Proxies. In *Late Cenozoic Paleoceanography, Developments in Marine Geology*. Hillaire-Marcel C, De Vernal A (eds) Elsevier B.V: 99-137.
- St-Onge G, Piper DJW, Mulder T, *et al.* 2004. Earthquake and flood-induced turbidites in the Saguenay Fjord (Québec): A Holocene paleoseismicity record. *Quaternary Science Reviews* **23** : 283–294.
- St-Onge G, Mulder T, Francus P, *et al.* 2007. Continuous physical properties of cored marine sediments. In *Proxies in Late Cenozoic Paleoceanography*. Hillaire-Marcel C, De Vernal A (eds) Elsevier B.V: 63-98.
- St-Onge G, Stoner J.S. 2011. Paleomagnetism near the North Magnetic Pole : a unique vantage point to understand the dynamics of the geomagnetic field and its secular variations. *Oceanography* **24** : 42-50.
- St-Onge G, Chapron E, Mulsow S, *et al.* 2012. Comparison of earthquake-triggered turbidites from the Saguenay (Eastern Canada) and Reloncavi (Chilean margin) Fjords : implications for paleoseismicity and sedimentology. *Sedimentary Geology* **243–244** : 89-107.
- Stuiver M, Polach HA. 1977. Discussion: reporting of ^{14}C data. *Radiocarbon* **19** : 355-363.
- Stuiver M, Reimer PJ, *et al.* 2005. CALIB 5.0. Available from <http://radiocarbon.pa.qub.ac.uk/calib/>.
- Tang CCL, Ross CK, Yao T, *et al.* 2004. The circulation, water masses and sea-ice of Baffin Bay. *Progress in Oceanography* **63** : 183–228.
- Tauxe L. 1993. Sedimentary records of relative paleointensity of the geomagnetic field in sediments: theory and practice, *Reviews of Geophysics* **31** : 319-354.

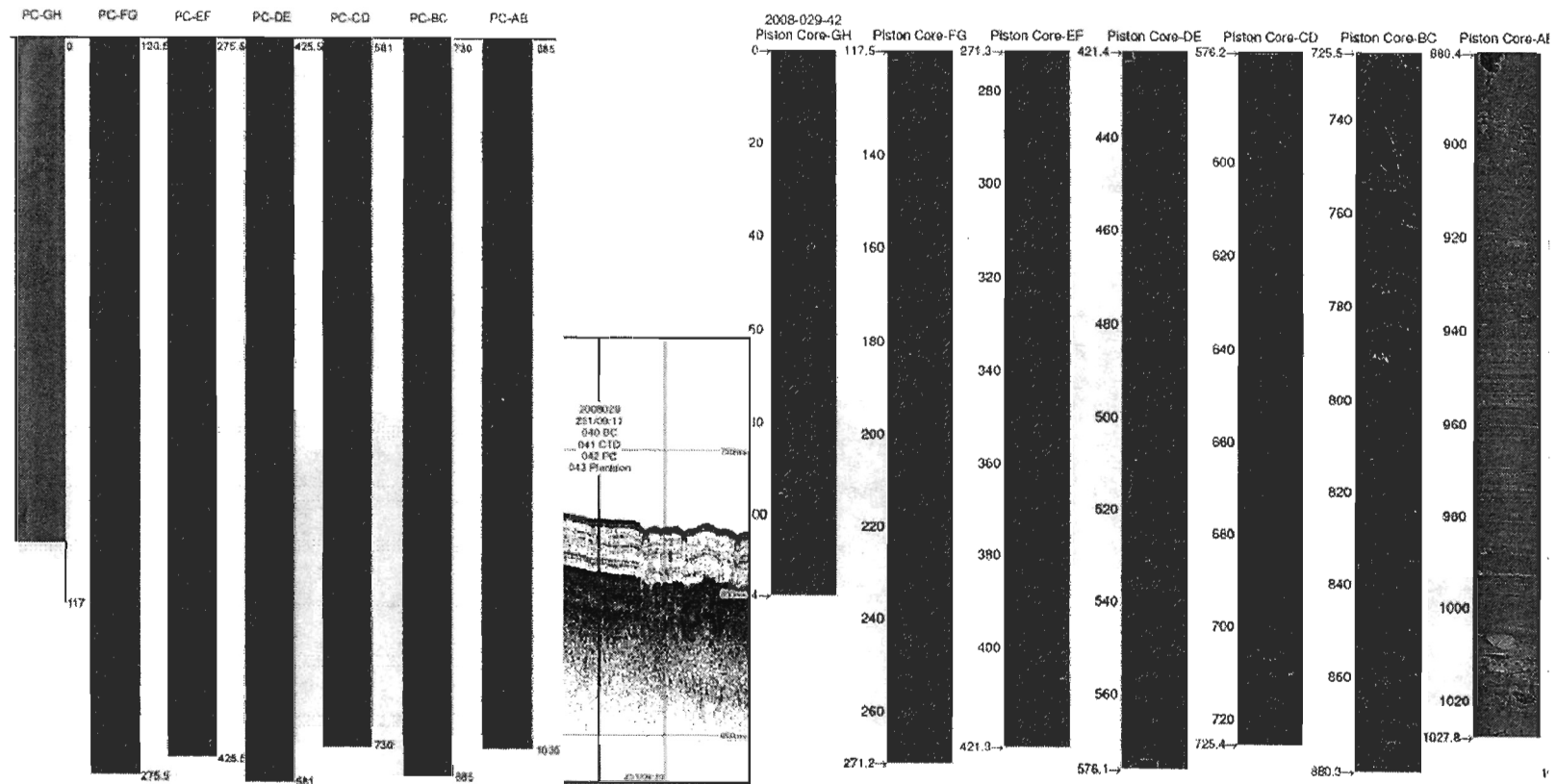
- Tauxe L, Kent DV. 2004. A simplified statistical model for the geomagnetic field and the detection of shallow bias in paleomagnetic inclinations: Was the ancient magnetic field dipolar? In *Timescales of the Paleomagnetic field* Channell, JET. et al. (eds). Geophysical Monograph Series: 145, 101-116.
- Tauxe L. 2010. *Essentials of Paleomagnetism*. University of California Press.
- Thompson R, Oldfield F. 1986. *Environmental Magnetism*. George Allen and Unwin Ltd: London.
- Wanner H, Solomina O, Grosjean M, Stefan, et al. 2011. Structure and origin of Holocene cold events. *Quaternary Science Reviews* 30: 3109-3123.
- Weeks R, Laj C, Endignoux L, Fuller M, Roberts A, Manganne R, Blanchard E, Goree W. 1993. Improvements in long-core measurement techniques: applications in palaeomagnetism and palaeoceanography. *Geophysical Journal International* 114: 651–662.
- Weidick A, Bennike, O. 2007. Quaternary glaciation history and glaciology of Jakobshavn Isbræ and the Disko Bugt region, West Greenland: a review. In *Geological Survey of Denmark and Greenland Bulletin* 14. Geological Survey of Denmark and Greenland (eds).

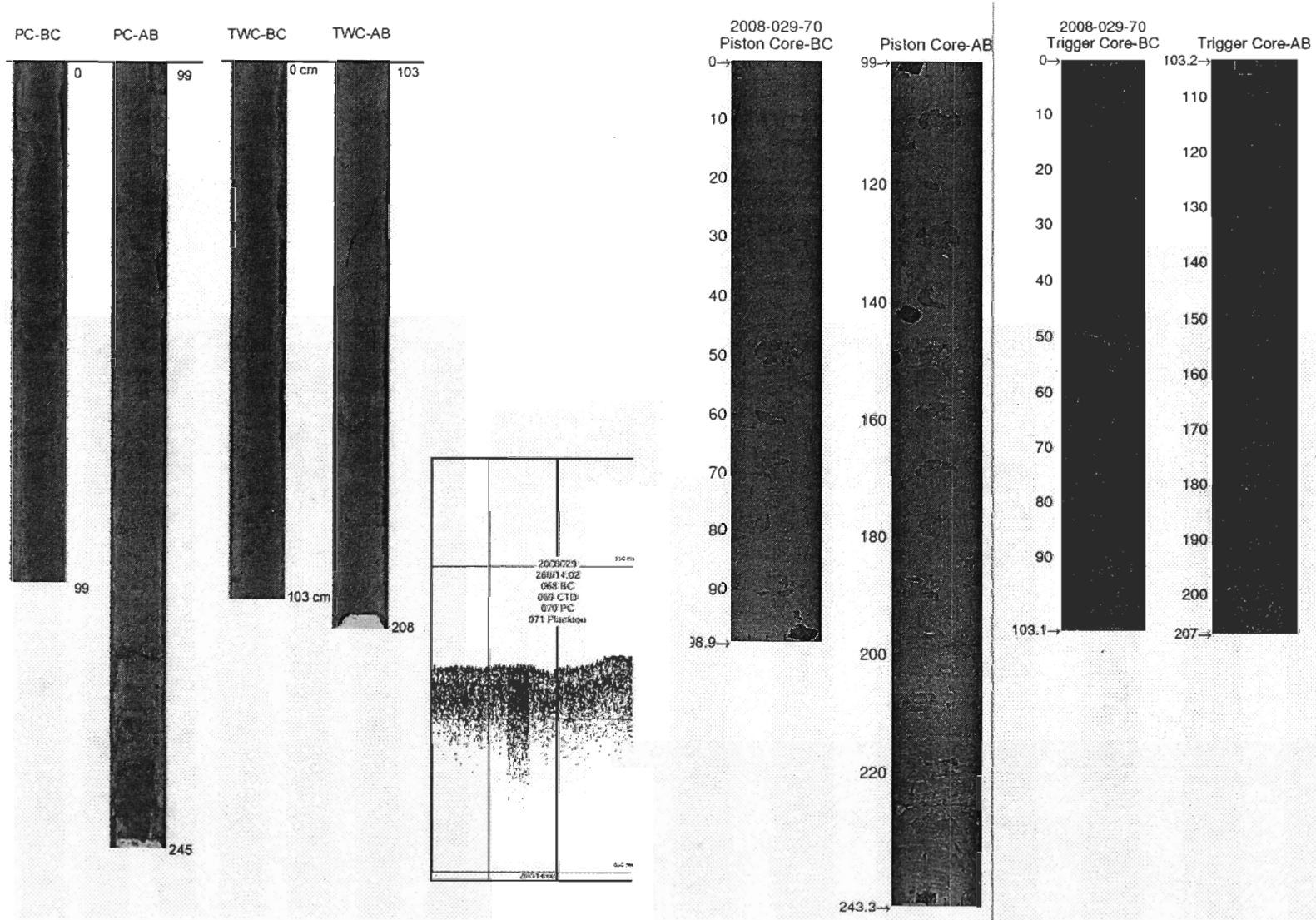
Background dataset

Supplementary data associated with this article can be found, in the online version at...









CHAPITRE 2

CONCLUSION GÉNÉRALE

Les faciès sédimentaires observés dans les quatre carottes de cette étude constituent des enregistrements des grands changements climatiques de l’Holocène dans la baie de Baffin. À l’exception de la carotte 38, dont le modèle d’âge ne remonte pas aussi loin, les autres carottes montrent des dépôts liés à la fonte des calottes glaciaires Inuitienne et Groenlandaise. Aussi, un signal sédimentaire associé au maximum climatique de l’Holocène a été observé dans toutes les carottes. De plus, des faciès sédimentaires correspondant à des événements climatiques locaux ont été mis en évidence sur les carottes 38 et 70. En comparant ces résultats à d’autres provenant des mêmes secteurs de la Baie de Baffin, il a été possible de bien décrire les changements océanographiques ayant eu lieu depuis environ 12000 ans.

De plus, des particularités environnementales locales ont été observées. Dans la carotte 38, un faciès associé à un événement froid de la période néoglaciale a été identifié de 2200 à 3700 a cal BP. Les signaux de cet événement ont été trouvés seulement de façon locale et non pas globale (Wanner *et al.*, 2011). Ceci indique donc que le Nord de la baie de Baffin (76°N), à l’embouchure de Nares Strait, a été affecté par cet épisode de froid engendré par une faible activité solaire (Wanner *et al.*, 2011). À Disko Bugt, un autre événement local a été identifié. Une turbidite datée à environ 2000 a cal BP pourrait être associée à un épisode de vêlage d’icebergs qui se serait produit à 2100 a cal BP (Andresen *et al.*, 2010). L’identification de ces particularités régionales montre que les propriétés physiques et magnétiques sont de bons indicateurs de changement environnementaux globaux et locaux. Le premier objectif de cette maîtrise, c'est-à-dire de décrire et interpréter des unités sédimentaires associées à des changements environnementaux durant l’Holocène a donc été atteint.

Ce mémoire de maîtrise a aussi permis de reconstituer les variations d'orientation du champ magnétique terrestre durant l'Holocène et d'en décrire la variabilité. En comparant les résultats de cette étude avec d'autres provenant de l'Arctique, il a été montré, qu'à des échelles millénaires et séculaires, le comportement du champ magnétique est enregistré de façon similaire dans l'Ouest et l'Est de l'Arctique Canadien. Cette découverte ouvre la voie à une plus grande utilisation des résultats paléomagnétiques comme outil de chronostratigraphie. En effet, en ayant peu ou pas de matériel à dater dans une carotte, il est tout de même possible de construire un modèle d'âge en corrélant les courbes d'inclinaison, de déclinaison et de paléo-intensité relative avec celles d'une carotte ayant un modèle d'âge robuste (Lisé-Pronovost *et al.*, 2009; Barletta *et al.*, 2008). Sachant que les variations millénaires et séculaires sont enregistrées similairement à la grandeur de l'Arctique canadien, cela permet l'utilisation d'un plus grand nombre de carottes de références à des fins de datation.

L'objectif deux, qui était de reconstruire et décrire la variabilité du champ magnétique terrestre à partir des quatre carottes sédimentaires afin de placer les changements actuels dans un contexte temporel plus important, a été réalisé pour trois des quatre carottes à l'étude. Mais l'observation des similitudes pour l'Est et l'Ouest de l'Arctique et ses implications à des fins de chronostratigraphie reste la découverte paléomagnétique majeure de cette maîtrise.

RÉFÉRENCES BIBLIOGRAPHIQUES

- Andresen C, David JS, McCarthy C *et al.* 2010. Interaction between subsurface ocean waters and calving of the Jakobshavn Isbræ during the late Holocene. *The Holocene* **21**: 221–224.
- Barber D, Marsden R, Minnett P. 2001a. Preface: The international North Water (NOW) polynya study. *Atmosphere-Ocean* **39** : 1.
- Barber D, Marsden R, Minnett P *et al.* 2001b. Physical processes within the North Water (NOW) polynya. *Atmosphere-Ocean* **39** : 163-166.
- Barletta F, St-Onge G, Channell JET, *et al.* 2008. High-resolution paleomagnetic secular variation and relative paleointensity records from the western Canadian Arctic: implication for Holocene stratigraphy and geomagnetic field behaviour. *Canadian Journal of Earth Sciences* **45** : 1265–1281.
- Barletta F, St-Onge G, Stoner JS, *et al.* 2010. A high-resolution Holocene paleomagnetic secular variation and relative paleointensity stack from eastern Canada. *Earth and Planetary Science Letters* **298** : 162-174.
- Brachfeld S. 2007. Relative Paleointensity in Sediments, In *Encyclopedia of Geomagnetism and Paleomagnetism*, Gubbins D, Herrero-Bervera E (eds), Springer Kluwer Press.

- de Vernal A, Rochon A. 2011. Dinocysts as tracers of sea-surface conditions and sea-ice cover in polar and subpolar environments. *IOP Conference Series: Earth and Environmental Science* **14** : 012007.
- Gogorza CSG, Lirio JM, Nuñez H, et al. 2004 Paleointensity studies on Holocene–Pleistocene sediments from lake Escondito Argentina. *Physics of the Earth and Planetary Interiors* **145** : 219–238.
- Gregory JM, Huybrechts P, Raper SCB. 2004. Threatened loss of the Greenland ice-sheet. *Nature* **428** : 616.
- Hanna E, Huybrechts P, Steffen K, et al. 2008. Increased Runoff from Melt from the Greenland Ice Sheet: A Response to Global Warming. *Journal of Climate* **21**: 331–341.
- Intergovernmental Panel on Climate Change (IPCC). 2007. Contribution of Working Groups I, II and III to the Fourth Assessment Report of the Intergovernmental Panel on Climate Change. Core Writing Team, Pachauri RK, Reisinger A (eds). IPCC : Geneva, Switzerland.
- Ingram RG, Bâcle J, Barber DG, Gratton Y, Melling H. 2002. An overview of physical processes in the NorthWater. *Deep Sea Research Part II: Topical Studies in Oceanography* **49**: 4893–4906.
- Jennings AE, Sheldon C, Cronin TM, et al. 2011. The Holocene history of Nares Strait: Transition from glacial bay to Arctic-Atlantic throughflow. *Oceanography* **24** : 26–41.
- Kelly MA, Lowell TV. 2009. Fluctuations of local glaciers in Greenland during latest Pleistocene and Holocene time. *Quaternary Science Reviews* **28**: 2088–2106.

- Knudsen KL, Stabell B, Seidenkrantz MS, *et al.* 2008. Deglacial and Holocene conditions in northernmost Baffin Bay: sediments, foraminifera, diatoms and stable isotopes. *Boreas* **37** : 346-376.
- Korte M, Genevey A, Constable CG, *et al.* 2005. Continuous geomagnetic field models for the past 7 millennia: 1. A new global data compilation, *Geochemistry Geophysics Geosystems* **6**: Q02H15.
- Levac E, de Vernal A, Blake WJ. 2001. Sea-surface conditions in northernmost Baffin Bay during the Holocene: palynological evidence. *Journal of Quaternary Science* **16** : 353–363.
- Li G, Piper DJW, Campbell C. 2011. The Quaternary Lancaster Sound trough-mouth fan, NW Baffin Bay. *Journal of Quaternary Science* **26**: 511–522.
- Lisé-Pronovost A, St-Onge G., Brachfeld S, *et al.* 2009. Paleomagnetic constraints on the Holocene stratigraphy of the Arctic Alaskan margin. *Global and Planetary Change* **68** : 85-99.
- Lloyd JM, Parka LA, Kuijpers A, *et al.* 2005. Early Holocene palaeoceanography and deglacial chronology of Disko Bugt, West Greenland. *Quaternary Science Reviews* **24** : 1741–1755.
- Lloyd JM, Kuijpers A, Long A, *et al.* 2007. Foraminiferal reconstruction of mid- to late-Holocene ocean circulation and climate variability in Disko Bugt, West Greenland. *The Holocene* **17** : 1079-1091.
- MacLean B, Woodside J.M, Girouard, P. 1984. Geological and geophysical investigations in Jones Sound, District of Franklin. *Geological Survey of Canada* **84-1A**: 359-365.
- Mann ME, Zhang Z, Rutherford S, *et al.* 2009. Global signatures and dynamical origins of the little ice age and medieval climate anomaly. *Science* **326** : 1256-1260.

- Miller GH, Wolfe AP, Briner JP, et al. 2005. Holocene glaciations and climate evolution of Baffin Island, Arctic Canada. *Quaternary Science Review* **24**: 1703-1721.
- Münchow A, Melling H, Falkner KK. 2006. An observational estimate of volume and freshwater flux leaving the Arctic Ocean through Nares Strait. *Journal of Physical Oceanography* **36** : 2025-2041.
- Opdyke ND, Channell JET. 1996. *Magnetic stratigraphy*. Academic Press : San Diego, CA.
- Pharand D. 2007. The Arctic Waters and the Northwest Passage: A Final Revisit. *Ocean Development & International Law* **38** : 3-69.
- Stoner JS, Laj C, Channell JET, et al. 2002. South Atlantic and North Atlantic geomagnetic paleointensity stacks (0–80 ka): implications for inter-hemispheric correlation. *Quaternary Science Review* **21**: 1141-1151.
- St-Onge G, Stoner JS, Hillaire-Marcel C. 2003. Holocene paleomagnetic records from the St. Lawrence Estuary : centennial- to millennial-scale geomagnetic modulation of cosmogenic isotopes. *Earth and Planetary Science Letters* **209** : 113-130.
- St-Onge G, Stoner J.S. 2011. Paleomagnetism near the North Magnetic Pole : a unique vantage point to understand the dynamics of the geomagnetic field and its secular variations. *Oceanography* **24** : 42-50.
- Tang CCL, Ross CK, Yao T, et al. 2004. The circulation, water masses and sea-ice of Baffin Bay. *Progress in Oceanography* **63** : 183–228.
- Trouet V, Esper J, Graham NE, et al. 2009. Persistent positive North Atlantic Oscillation Mode Dominated the Medieval Climate Anomaly. *Science* **324** : 78-80.
- Wanner H, Solomina O, Grosjean M, Stefan, et al. 2011. Structure and origin of Holocene cold events. *Quaternary Science Reviews* **30**: 3109-3123.

- Weidick A, Bennike, O. 2007. Quaternary glaciation history and glaciology of JakobshavnIsbræ and the DiskoBugt region, West Greenland: a review. In *Geological Survey of Denmark and Greenland Bulletin 14*. Geological Survey of Denmark and Greenland (eds).
- Yamazaki T, Oda H. 2005. A geomagnetic paleointensity stack between 0.8 and 3.0 Ma from equatorial Pacific sediment cores. *Geochemistry Geophysics Geosystems* **6** : Q11H20.
- Zhang X, Walsh JE. 2006. Toward a seasonally ice-covered Arctic Ocean: Scenarios from the IPCC AR4 model simulations. *Journal of Climate* **19** : 1730– 1747.

